https://doi.org/10.5194/wes-2026-136
Preprint. Discussion started: 7 August 2026
© Author(s) 2026. CC BY 4.0 License.

WIND ENERGY SCIENCE DISCUSSIONS

Leading-edge erosion risk: Assessment of uncertainties

Charlotte Bay Hasager, Abhiram Vinod, Laurids Dencker Di Stefano Toft, Krystallia Dimitriadou

Department of Wind and Energy Systems, Technical University of Denmark, Frederiksborgvej 399, 4000 Roskilde, Denmark

Correspondence to: Charlotte Hasager (cbha@dtu.dk)

Abstract. Leading-edge erosion of wind turbine blades due to hydrometeor impacts is observed across various climate zones. This study focuses on uncertainties in the assessment of end of incubation (EoI) and erosion-safe operation (ESO) efficiency using different types of meteorological observations. At the Risø site in Denmark the following data are retrieved: a 19-year-long time series from a rain gauge and a cup anemometer, up to 3-year long time series from disdrometers and a sonic, and 10-year-long satellite-based product IMERG (Integrated Multi-satellitE Retrievals for Global Precipitation Measurement) and modeled wind speed from NEWA (New European Wind Atlas). The Spearman coefficient between joint precipitation and wind speed time series consistently takes positive values across the time series. Three reference turbines are assumed to have been installed at Risø. An impingement damage model derived from a rain erosion test is used to assess EoI and ESO efficiency. Key results on the uncertainty in assessing EoI are: 1) a long series is recommended, as EoI from 1-year time series varies by ~170% between the minimum and maximum EoI. Uncertainty in EoI due to the choice of droplet slowdown is ~24% when comparing an advanced model and the DNV Recommended Practice. Disdrometers estimate longer EoI than rain gauge due to under catch and missing data. The intuitive perception that similar EoI will occur across all blades of a turbine or within a wind farm exposed to the same weather is rarely observed in the field. Probabilistic variations in EoI are assessed using Monte Carlo simulations of the Pareto fronts for weather and materials. It is found that the uncertainty due to the material is larger than that due to the weather. The combined effect explains why the intuitive perception does not hold for EoI. ESO efficiencies are assessed from Pareto fronts. A flat Pareto front indicates high ESO efficiency, with only a small amount of AEP lost to ensure a long EoI extension. High-frequency disdrometer data (1-minute) with good measurement resolution (0.1 mm h^{-1}) show flatter Pareto fronts than IMERG data (30-minute, 0.1 mm h^{-1}). Resampling disdrometer data from 1-minute to 30-minute intervals results in steeper Pareto fronts, as expected, like those of IMERG. Rain gauge observations are inadequate due to limited measurement resolution (1.2 mm h^{-1}). ESO efficiency is affected by the choice of droplet slowdown model, with the advanced model yielding flatter Pareto fronts. A recommendation is to assess the relevance of EoI from long-term time series and, in synergy with high-frequency observations, assess ESO efficiency for operational decision making.

1 Introduction

https://doi.org/10.5194/wes-2026-136
Preprint. Discussion started: 7 August 2026
© Author(s) 2026. CC BY 4.0 License.

In 2025, the EU's electricity generation mix showed that 17% was produced by wind turbines (EMBER, 2026). Society is moving towards the electrification of industries, transport, heating, and data centers. More electricity will be needed for the transition. A continued growth in the share of electricity from wind energy is expected in Europe (WindEurope, 2025) and worldwide (GWEC, 2025). Wind energy is a weather-driven energy source, with wind as the alpha and omega for ensuring electricity production. Weather, however, can bring precipitation that may pose a challenge for wind turbine blades.

Wind turbine blade leading-edge erosion (LEE) is a weather-dependent phenomenon. Turbines with eroded blades experience a loss in annual energy production (AEP) compared to those with clean blades (Maniaci et al., 2022; Malik and Bak, 2025). Furthermore, turbine downtime for monitoring erosion status and repairing eroded blades causes AEP loss and increases operation and maintenance (O and M) costs (Mishnaevsky and Thomsen, 2020; Pryor et al., 2025). An adverse effect of LEE is microplastic emission, though three orders of magnitude smaller than emission from tires (Mishnaevsky et al., 2024).

Wind turbines operate across a wide range of climatic conditions, characterized by variations in wind speed and precipitation in both space and time. LEE is primarily driven by the impact of hydrometeors on blades when turbines operate at or near rated speed. The impact velocity between a rain droplet or hailstone and the leading edge of a blade is a function of the revolutions per minute (rpm) and the length of the rotor blade, i.e., the tangential velocity. However, the impact velocity (closing velocity) is smaller than the tangential velocity due to aerodynamic interactions between the droplet field and the airfoil (Papadakis et al., 2007; Prieto and Karlsson, 2021; Castorrini et al., 2024). The aerodynamic interaction causes droplet slowdown as a function of droplet size and airfoil shape (Barfknecht and von Terzi, 2024). Impact efficiency is included in the recommended practice (RP) by DNV (DNV, 2021).

The DNV PR quantifies the relationship between damage progression from known droplet sizes and impact velocities for a leading-edge protection (LEP) system, using the whirling arm rain erosion tester (RET) (DNV, 2021). RET data analysis provides estimates of the time to end of incubation (EoI), i.e., the onset time of visible damage. The LEP systems suitable for wind turbines exhibit a logarithmic dependence, with greater damage at higher velocities.

RET data from an experiment with four droplet sizes and several rotational speeds, ranging from 90 to 150 m s^{-1}, formed the basis of the impingement model by Bech et al. (2022). The impingement model sums up the amount of water (water column) impacting the blade and integrates cumulative stress using the Palmgren-Miner's summation. At each time step with impinged water, additional stress is added, and a damage increment is counted (ASTM, 2021). The estimation of blade lifetime for a wind turbine is based on a time series of concurrent measurements of wind speed and rain rate.

Investigations into the co-variation of rain and wind data at high temporal resolution show rain-wind speed dependencies impacting the assessment of erosion progression in a variety of environments, including land and sea (e.g., Hasager et al. 2021; Verma et al., 2021a; Castorrini et al., 2024; Pryor et al., 2025; Visbech et al., 2025). The DNV RP assumes the rain and wind data are constant and independent of events over time (DNV, 2021). Studies have shown that this assumption yields a shorter estimate of the time to EoI than using synchronized rain and wind observations, e.g., in the Netherlands (Verma et al., 2021b) and in the UK (Castorrini et al., 2024; Visbech et al., 2025; Simon et al., 2026).

https://doi.org/10.5194/wes-2026-136
Preprint. Discussion started: 7 August 2026
© Author(s) 2026. CC BY 4.0 License.

Several studies on LEE are based on rain gauge data, e.g., in Ireland, the US, the Netherlands, Spain, and Denmark (Nash et al., 2021; Pryor et al., 2025; Verma et al., 2021a; Dimitriadou et al., 2024; Hasager et al., 2020), among other countries. In contrast to rain gauges used by meteorological agencies to monitor precipitation for decades, disdrometers, which observe drop-size distribution and fall velocities of hydrometeors, are of more recent origin and far fewer in number. The LEE assessment based on disdrometer data includes land sites in Denmark, the UK, and the US (Hannesdottír et al., 2024a; Castorrini et al., 2024; Letson and Pryor, 2023) and offshore, coastal, and inland sites in the Netherlands (Caboni et al., 2024; Caboni and van Dalum, 2025) among other countries.

Rain gauge data often span decades. Examples of LEE studies based on long rain gauge data time series encompassing 50 years (Verma et al., 2021b), 30 years (Nash et al., 2021), up to 28 years (Hasager et al., 2024), and 18 years (Pryor et al., 2025), while LEE studies based on disdrometer time series often are shorter than 5 years. The advantage of a disdrometer is the high temporal resolution, while a disadvantage is the lack of long-term data.

A long-term goal is to characterize LEE risk across several climate zones on land and at sea in Europe using standardized, long-term wind speed and rainfall rate data from selected wind-energy-relevant sites. In contrast to the Contiguous US, which maintains a nationwide network of local observations of rain rate every 1 minute and wind speed every 5 minutes over 18 years at more than 880 stations (Pryor et al., 2025), Europe lacks similar standardized, granular wind speed and rain data. In Europe, a standardized precipitation product based on weather station time series observations is E-OBS, available as daily gridded precipitation amounts at a spatial resolution of 0.1 degrees, not differentiating between liquid (rain) and solid precipitation (snow and hail), and excluding offshore areas (Cornes et al., 2018).

One option to provide spatial coverage is to use numerical model precipitation results from reanalyses, mesoscale models, or large eddy simulations. LEE assessment in various countries based on various numerical models and different lengths of time series includes, e.g., a mesoscale model for Japan for 10 years (Sakai et al., 2026), a mesoscale model for Northern Europe for 8 years (Visbech et al., 2023), reanalysis and mesoscale model for Scandinavia for 5 years (Hannesdóttir et al., 2024a), and mesoscale model and large eddy simulation for the Netherlands for 10 years and 1 year, respectively (Caboni and Dalum, 2025).

Another option for providing spatial coverage is to use satellite-based precipitation observations from GPM IMERG. GPM stands for the Global Precipitation Measurement satellite mission, and IMERG stands for Integrated Multi-satellitE Retrievals for GPM (Huffmann et al., 2023). The IMERG product has been widely validated and is considered one of the most reliable global satellite precipitation datasets, particularly for capturing large-scale spatial patterns, seasonal cycles, and extremes (Pradhan et al., 2022). The Final Run product gauge adjustment monthly (GPCC, 2026) generally shows the highest accuracy, reducing systematic bias compared with earlier runs, though performance varies regionally, with challenges over complex terrain, in arid regions, in high latitudes, and in snowfall-dominated areas (Yu et al., 2022; Wang et al., 2022). The gauge adjustment is monthly (NCAR Staff, 2026). Evaluations across continents, including China, the Tibetan Plateau, and the US, show strong agreement with gauge data at daily and monthly scales. However, light precipitation and fine-scale retrievals remain less accurate. Overall, IMERG is suitable for hydrological, climatological, and environmental applications when regional limitations are taken into account (Pradhan et al., 2022; Gao et al., 2025). The IMERG precipitation estimates can be separated into probabilistic contributions from liquid and solid hydrometeors, reflecting the likelihood of each precipitation type.

The accuracy of IMERG has been evaluated for parts of Europe. A comparison study between E-OBS and higher-temporal-resolution data sources shows that IMERG correlates better with E-OBS than other satellite-based products in the Mediterranean Region (Retalis et al., 2022). A comparison study by Varga and Breuer (2023) between E-OBS and other datasets covering south-east Central Europe shows that IMERG correlates better with E-OBS than the ERA5 reanalysis (Hersbach et al., 2020) and the Weather Research and Forecasting (WRF) mesoscale model (Skamarock et al., 2019). Precipitation observations at three coastal sites in Belgium showed a higher correlation with IMERG than with ERA5 and NORA3 (Ivanova, 2025). NORA3 is the Norwegian reanalysis (Haakenstad et al., 2021; Solbrekke et al., 2021).

The EoI has been estimated using IMERG rainfall and local observations of rainfall and wind in Denmark, Norway, Germany, and Portugal (Badger et al., 2022). IMERG and local precipitation observations in Navarra, Spain, have been compared and used in combination with wind speed from the New European Wind Atlas (NEWA) (NEWA, 2026) to estimate EoI (Dimitriadou et al., 2024; Dimitriadou and Hasager, 2026). EoI has been investigated using IMERG rainfall over the British Isles and surrounding seas, collocated with NEWA wind speeds (Visbech et al., 2025).

Convective precipitation over Europe, quantified from IMERG and other sources for a 10-year climatology, shows that up to 10% of total annual precipitation is convective over land, while up to 40% is convective over sea. Convective precipitation prevails primarily during summer in continental Europe and the coastal North Sea, Baltic Sea, and northern Adriatic Sea, while during winter in southern Europe and the Mediterranean Sea. Convective precipitation is defined as a precipitation rate ≥ 10 mm h^{-1}, and lightning flashes occur within a 20-km distance. Convective precipitation is typically short-lived, and high-temporal-resolution meteorological data are needed to quantify these events.

Heavy rain combined with high winds results in many heavy droplets impacting blades at high impact velocity over short time intervals, leading to erosion. The total period of such conditions may vary from a few hours to several days per year, depending on site and weather variability, e.g., 56 hours in the Southern Great Plains contributes around half of the time to EoI (Pryor and Barthelmie, 2025), and in the Dutch North Sea, around 30% of yearly damage in just over 12 hours (Caboni et al., 2024).

The hypothesis that erosion-safe operation (ESO), which involves applying wind turbine control to reduce the impact velocity of hydrometeors during intense rain events, could reduce LEE with limited loss of annual energy production (AEP) was proposed by Bech et al. (2018). Further studies include the economic perspective of ESO, including spot market electricity costs (Skrzypiński et al., 2020), cost of capital expenditures and repair (Letson and Pryor, 2023), average electricity costs (Pryor and Barthelmie, 2026), postponement of repair needs using ESO optimized with reinforcement learning at wind farm scale (Visbech et al., 2024), aerodynamic consideration of ESO (Castorrini et al., 2024), and the site suitability of ESO characterized by the long-term site-specific rainfall and wind speed data (Visbech et al., 2025). Erosion-safe operation efficiency quantifies the relationship between the expected extended lifetime for expected AEP loss values. For short-lived rain events during high winds, curtailing the turbines only during the short events limits AEP losses compared to using, e.g.,

https://doi.org/10.5194/wes-2026-136
Preprint. Discussion started: 7 August 2026
© Author(s) 2026. CC BY 4.0 License.

30-minute intervals. The implementation of ESO at wind farms is expected to rely on minute-scale rainfall data to avoid unnecessary AEP losses (Tilg et al., 2020). Barfknecht et al. (2024) investigated ESO at sites in the Netherlands using weather radar for now casting.

The objective of the current study is to investigate the uncertainty in erosion risk assessment of EoI and ESO efficiency across different meteorological data types. This work lays the foundation for a future goal of mapping erosion risk across Europe to support decision-making in the wind industry.

The structure of the paper comprises the presentation of the site and data in Section 2, the method for assessing EoI and ESO efficiency in Section 3, followed by the results, discussion, and conclusion in Sections 4, 5, and 6, respectively.

2 Data and methods

2.1 Study area and meteorological observations

The study covers the DTU Risø campus in Denmark, located on the Roskilde Fjord. The geographical coordinates are latitude 55,694°N, and longitude 12,088°E, elevation 0 m. The study area is indicated in Fig. 1. An overview of the data sources is listed in Table 1.

https://doi.org/10.5194/wes-2026-136
Preprint. Discussion started: 7 August 2026
© Author(s) 2026. CC BY 4.0 License.

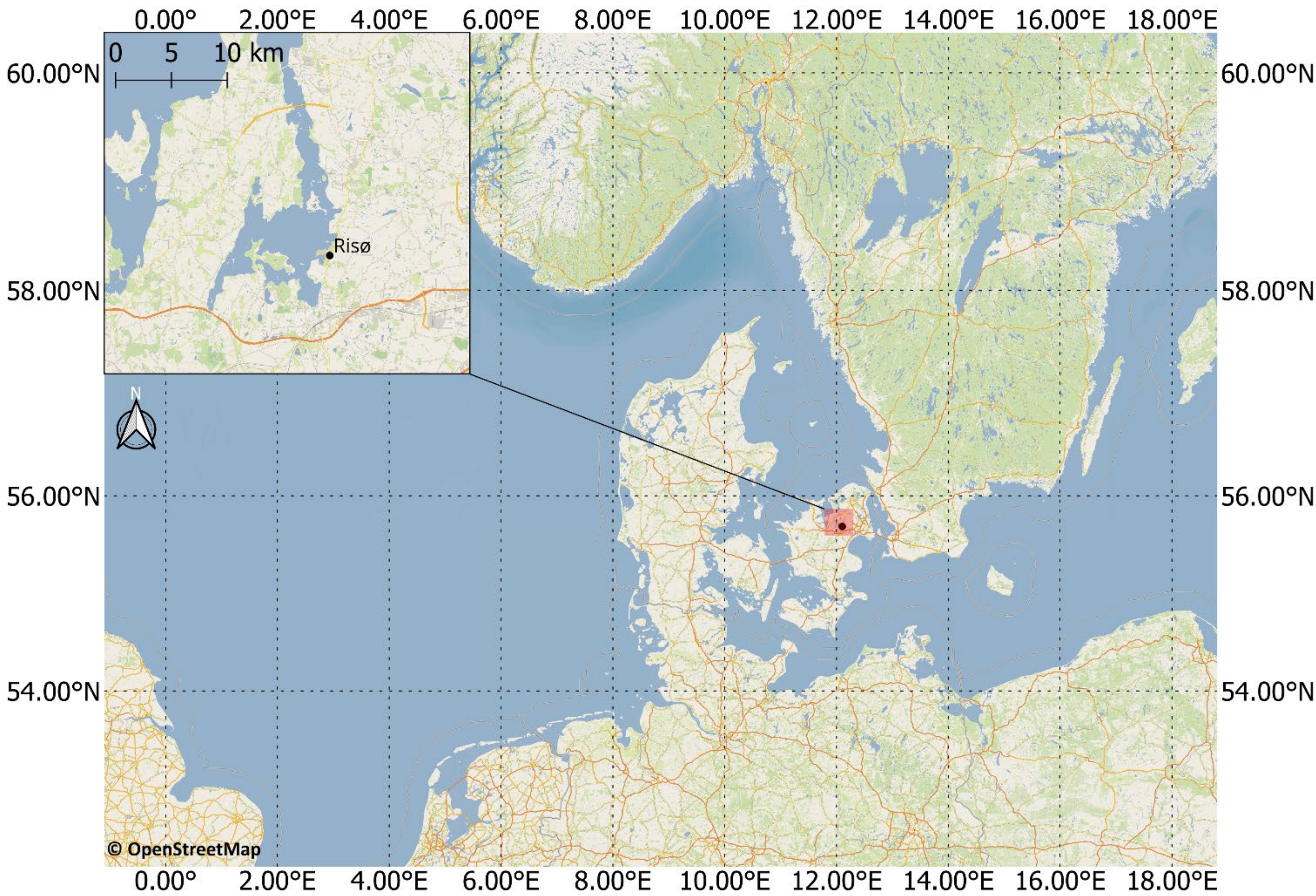

150 Figure 1. Location of the DTU Risø campus study site. Map layer credit: OpenStreetMap https://www.openstreetmap.org.

Table 1. Overview of meteorological data sources used in the analysis.

Parameter	Source	Temporal resolution (minutes)	Spatial resolution (km)	Observation height (m)	Length of period (years)
Wind speed	Cup anemometer	10	Point	125	19
	Sonic	1	Point	60	3
	NEWA	30	3	50, 75, 100, 150	10
Precipitation rate	Rain gauge	10	Point	0	19
	Parsivel^2	1	Point	0	3
	Parsivel^2 top	1	Point	123	2
	Thies	1	Point	0	2
	IMERG	30	11	0	10

https://doi.org/10.5194/wes-2026-136
Preprint. Discussion started: 7 August 2026
© Author(s) 2026. CC BY 4.0 License.

WIND ENERGY SCIENCE DISCUSSIONS

Precipitation data from a heated tipping-bucket rain gauge (RIMCO) with 0.2 mm per 10 min (1.2 mm h^{-1}) resolution during recent decades at the Risø site are available. Precipitation data stored at 10-minute resolution is selected. The rain gauge is located at the base of the tall meteorological mast at Risø. Precipitation observed from two disdrometers of type Parsivel^2 Laser Present Weather Sensor (OTT Instruments) during recent years at Risø site with 0.1 mm h^{-1} resolution and stored at 1-minute temporal resolution is selected. The Parsivel^2 installed near the rain gauge is subsequently called Parsivel^2 while the other installed at the top of the tall meteorological mast at a height of 123 m is subsequently called Parsivel^2 top (Mishnaevsky et al., 2021). Precipitation observed from a disdrometer of type Thies Laser Precipitation-Monitor (Thies Klima) (subsequently called Thies) is located near the rain gauge and Parsivel^2. Precipitation data observed at 0.1 mm h^{-1} resolution, stored at 1-minute resolution, is selected. Fig. 2 shows the precipitation sensors at the ground and the met mast.

Figure 2. Photos from left Parsivel^2 and Thies, rain gauge, and meteorological mast at Risø site.

Wind speed observations from cup anemometers (Risø P2546A, WindSensor Aps, Denmark) mounted on 6m-long booms at 225 degrees at several heights and at the top of the tall meteorological mast are available over recent decades. The cup anemometers were calibrated in a wind tunnel prior to operation. Wind speeds at 125m height at the top of the mast, stored at 10-minute resolution, are selected for the period 2002 to 2025. A shorter series from 2012 to 2025 from 118m height is also selected. Wind speed observations from sonic anemometers (Metek USA) mounted on 6m-long booms at several heights on the mast are available over recent decades. Wind speeds at 60m height, stored at 1-minute resolution, are selected. The time series is filtered, retaining high-quality data.

Observations of wind speed and precipitation rate from a cup anemometer at 125m and a rain gauge over 19 years are collocated at 10-minute resolution. In the absence of missing data, there would be ~998640 collocated samples, whereas the data show ~952100 samples, i.e., 95% availability.

The data availability of collocated observations at 1-minute resolution from sonic and disdrometers is shown in Fig. 3. In the case of no missing data for one year, the number of samples is ~525600. Sonic data have high availability, while disdrometer data availability varies. To compare erosion risk assessments across all three disdrometers, our selection includes years with

https://doi.org/10.5194/wes-2026-136
Preprint. Discussion started: 7 August 2026
© Author(s) 2026. CC BY 4.0 License.

more than 400,000 samples (75% availability). Only 2021 fulfils the criteria for three disdrometers. Additional analysis based on Parsivel² and sonic data provides a three-year time series covering 2020, 2021, and 2023.

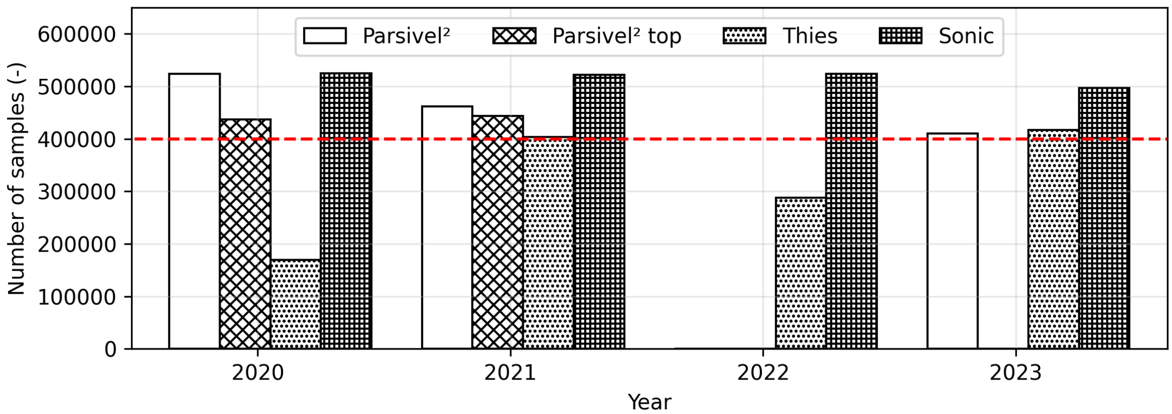

Figure 3. Number of samples from three disdrometers: Parsivel² and Thies on the ground near the meteorological mast, and Parsivel² top located at a height of 123 m on the mast. Sonic data are observed at a height of 60 m. The dashed line indicates the data selection threshold.

2.2 IMERG

The Global Precipitation Measurement Integrated Multi-satellite Retrievals (GPM IMERG) dataset provides global, gridded precipitation estimates at a spatial resolution of 0.1° and a temporal resolution of 30 minutes. These estimates are derived from an integrated constellation of passive microwave and infrared satellite sensors, including observations from the GPM Core Observatory and partner satellites, enabling near-global coverage and an improved representation of precipitation variability (Huffman et al., 2020, 2023).

The IMERG retrieval algorithms and input datasets are continuously refined as additional observations, improved calibration techniques, and enhanced retrieval methodologies become available. In this study, we employ the IMERG Final Run precipitation product (Version 07), which incorporates these advancements and applies a monthly gauge-based bias correction using quality-controlled in situ rain-gauge observations. Owing to its improved accuracy and stability, the Final Run Version 07 product is recommended for research applications and is therefore used in our analysis (Huffman et al., 2020, 2023).

This study used the IMERG V07 precipitation, *precipitationQualityIndex* field for the years 2014-2023, extracted for the Risø site location. The precipitation field provides calibrated precipitation estimates derived from combined infrared and microwave satellite observations. To ensure sufficient data quality, precipitation samples with a *precipitationQualityIndex* below 0.4 were excluded (Huffman et al., 2020). The time series at the Risø site showed near-zero data with low quality. Data availability is 100%.

https://doi.org/10.5194/wes-2026-136
Preprint. Discussion started: 7 August 2026
© Author(s) 2026. CC BY 4.0 License.

2.3 NEWA

The New European Wind Atlas (NEWA) provides high-resolution, openly accessible wind resource data across Europe, designed to support wind energy planning and research (NEWA, 2026). It combines advanced atmospheric modeling with extensive measurement campaigns to deliver detailed maps of wind speed, turbulence, and other key parameters at multiple heights. By improving the accuracy of wind assessments, especially in complex terrain and offshore environments, NEWA helps reduce uncertainty and risk in wind farm development (Dörenkämper et al., 2020). Hereby, we extracted NEWA wind speed data for the Risø site at the heights of 50, 75, 100, and 150 m for the years 2014-2023. Interpolation using the logarithmic wind profile is applied to calculate the wind speed at hub height.

3 Methods

3.1 End of Incubation (EoI)

The impingement damage model by Bech et al. (2022) is selected to assess EoI. Impingement of water on the blade at a given timestep causes stress on the blade, and a damage increment is counted. Using Palmgren-Miner's summation, the cumulative stress is integrated over the period. When the cumulative stress reaches 1, the EoI is reached. It is assumed that the blade will be repaired at this time, and a new cycle will begin.
The precipitation rates observed from rain gauges, disdrometers, and IMERG are assumed to follow the droplet size distribution and droplet fall velocity as given by Best (1950). In the damage model calculation, the weighted effect of droplets across the full size spectrum is used, following Madsen et al. (2026).
The impact speed of droplets on the leading edge is influenced by aerodynamic effects, which slow the droplets before impact. The slowdown is a function of droplet sizes and airfoil. The DNV Recommended Practice (DNV, 2021) suggests applying impingement efficiency as a function of hydrometeor diameter only. A more comprehensive aerodynamic slowdown model incorporates airfoil characteristics to provide a more detailed estimate of the energy impact (Barfknecht and von Terzi, 2024). Smaller droplets have impact efficiencies below 1. The non-linearity arising from variations in impact velocity during the rotor sweep of the blades is also included, accounting for the small increases in velocity that lead to exponential increases in erosion. The sensitivity analysis of the uncertainty in the assessment of EoI related to using one 'representative' year versus longer consecutive time periods is investigated using 19-year time series observations.

3.2 ESO efficiency (Pareto front)

https://doi.org/10.5194/wes-2026-136
Preprint. Discussion started: 7 August 2026
© Author(s) 2026. CC BY 4.0 License.

The efficiency of ESO (ESO_{eff}) is defined as the extension in damage accumulation (ΔD) relative to the AEP loss (ΔAEP_{loss}) defined as

$$ESO_{eff} = \frac{\Delta D}{\Delta AEP_{loss}} \qquad (1)$$

For normal operation, the turbine operates in all weather conditions. For ESO, curtailing the turbine during heavy rain events reduces damage. The optimal ESO depends on the weather, material, and turbine tip-speed curve. The method for assessing ESO efficiency, based on a continuous range of optimal strategies along the Pareto front, was developed by Madsen et al. (2026). A Pareto front represents the set of solutions for which no solution outperforms any other solution in the set. The set of solutions along the Pareto front provides an option for selecting the preferred balance between damage and AEP loss. Variability in precipitation rate, wind speed, and material impacts the ESO efficiency results.

A Monte Carlo-based approach for deriving probabilistic Pareto fronts was developed by Madsen et al. (2026). The method enables uncertainty analysis for weather and materials around the Pareto front. If only the uncertainty due to weather is assessed, the wind speed and precipitation rate data are randomly selected from a longer time series, based on one year of data. At the same time, the material properties are used deterministically. Alternatively, the uncertainty due to material is assessed by keeping the weather data deterministic and randomly selecting material properties. The total uncertainty from weather and materials is assessed using a Monte Carlo simulation, with weather and material data sampled randomly. It may be noted that variability in EoI is also seen for normal operation. In other words, not all blades at one turbine or all turbines within a wind farm will experience the same damage level in the given environment.

3.3 Turbine types

The turbine tip speed curve, hub-height, rotor diameter and the blade airfoil are relevant parameters. Three reference turbines, NREL 5MW (Jonkman et al., 2009), DTU 10 MW (Bak et al., 2013), and IEA 15 MW (Gaertner et al., 2020) are used in the study. Table 2 lists selected details.

Table 2. Wind turbines specifications.

Turbine	Hub height (m)	Rotor (m)	Cut-in ($m\ s^{-1}$)	Rated ($m\ s^{-1}$)	Cut-out ($m\ s^{-1}$)	Max. (rpm)	Max. tip speed ($m\ s^{-1}$)
NREL 5 MW	90	126	3	11.4	25	12.1	80
DTU 10 MW	119	178.3	4	11.4	25	9.6	90
IEA 15 MW	150	240	3	10.6	25	7.56	95

https://doi.org/10.5194/wes-2026-136
Preprint. Discussion started: 7 August 2026
© Author(s) 2026. CC BY 4.0 License.

The logarithmic wind profile assuming neutral conditions is applied to calculate wind speeds (u) at turbine hub height (h) from observation height (h_{obs}). The roughness length (z_0) is assumed to be 0.5 m.

$$u(h) = u(h_{obs}) \cdot \frac{\ln\left(\frac{h}{z_0}\right)}{\ln\left(\frac{h_{obs}}{z_0}\right)} \qquad (2)$$

4 Results

4.1 Weather conditions

The average annual precipitation, average annual wind speed, and their covariation, calculated using Spearman correlations and trendlines, are presented for the 19-year cup anemometer and rain gauge time series in Fig. 4. The time series spans from 2002 to 2025, with a gap from 2007 to 2012. A positive Spearman coefficient is observed, ranging from 0.025 to over 0.1. The trendline shows an increase driven by higher precipitation in later years.

Results based on NEWA and IMERG for 10 years from 2014 to 2023 are shown in Fig. 5. The Spearman correlation is positive for all years, ranging from 0.05 to more than 0.15. A positive trend in the Spearman coefficient is observed in this shorter time series.

Weather conditions observed by sonic and three disdrometers from 2020 to 2023, and calculated Spearman correlations show positive Spearman correlations ranging from 0.1 to more than 0.15 in Fig. 6.

Rain gauge data shows variations from ~400 to ~1000 mm yr^{-1}. IMERG shows from ~400 to ~800 mm yr^{-1}. Disdrometers show from ~350 to 600 mm yr^{-1}. The result indicates under catch in disdrometers, though 25% of missing data partly explains differences. Examining the accuracy of each sensor type is beyond our scope. High-quality sensor data is collected. Our focus is on uncertainties in the assessment of EoI and ESO efficiency based on available time series.

https://doi.org/10.5194/wes-2026-136
Preprint. Discussion started: 7 August 2026
© Author(s) 2026. CC BY 4.0 License.

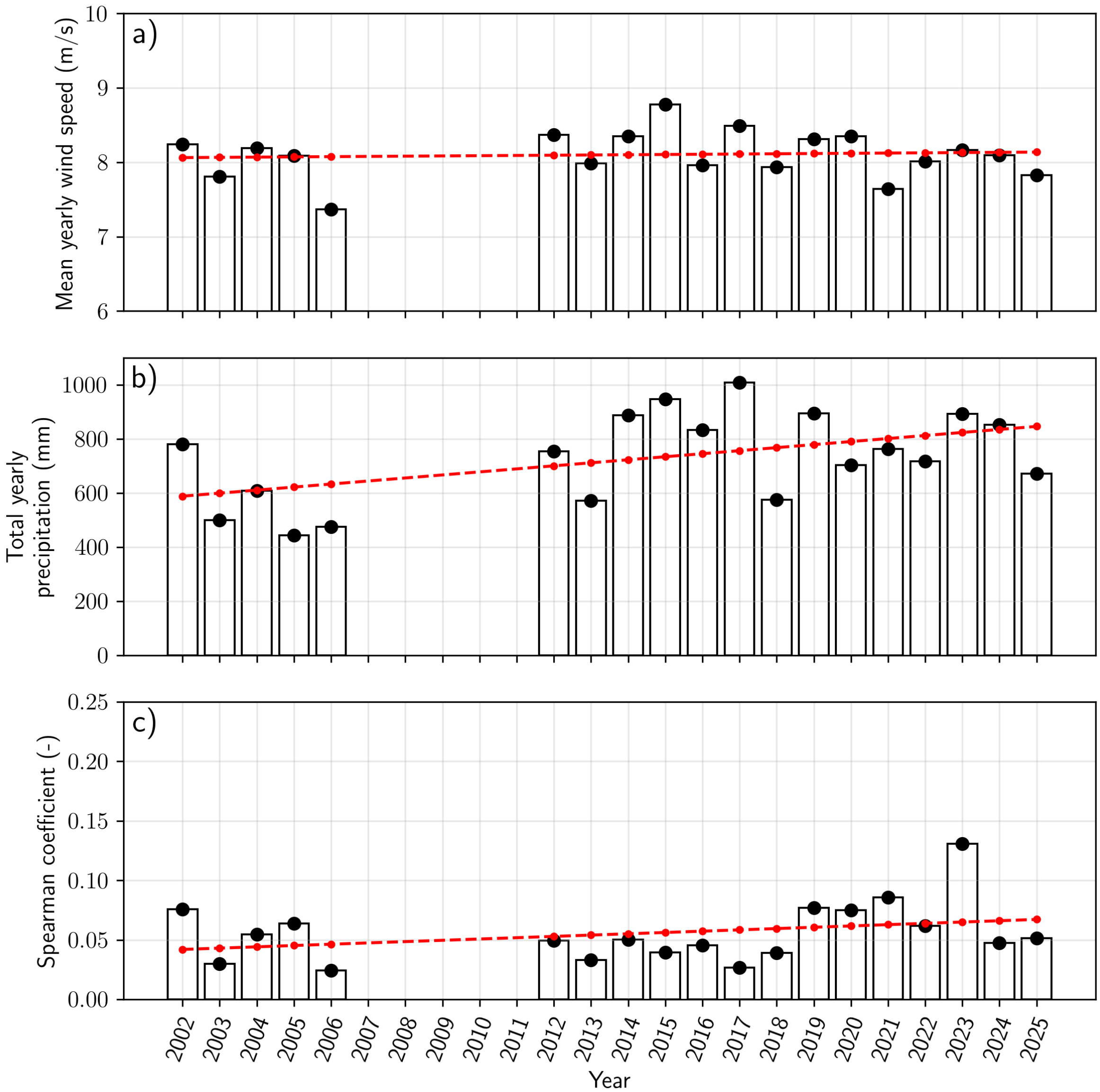

Figure 4. Mean yearly wind speed from cup anemometer at 125 m height, mean yearly precipitation from rain gauge and Spearman
290 **coefficient for Risø, DTU.**

https://doi.org/10.5194/wes-2026-136
Preprint. Discussion started: 7 August 2026
© Author(s) 2026. CC BY 4.0 License.

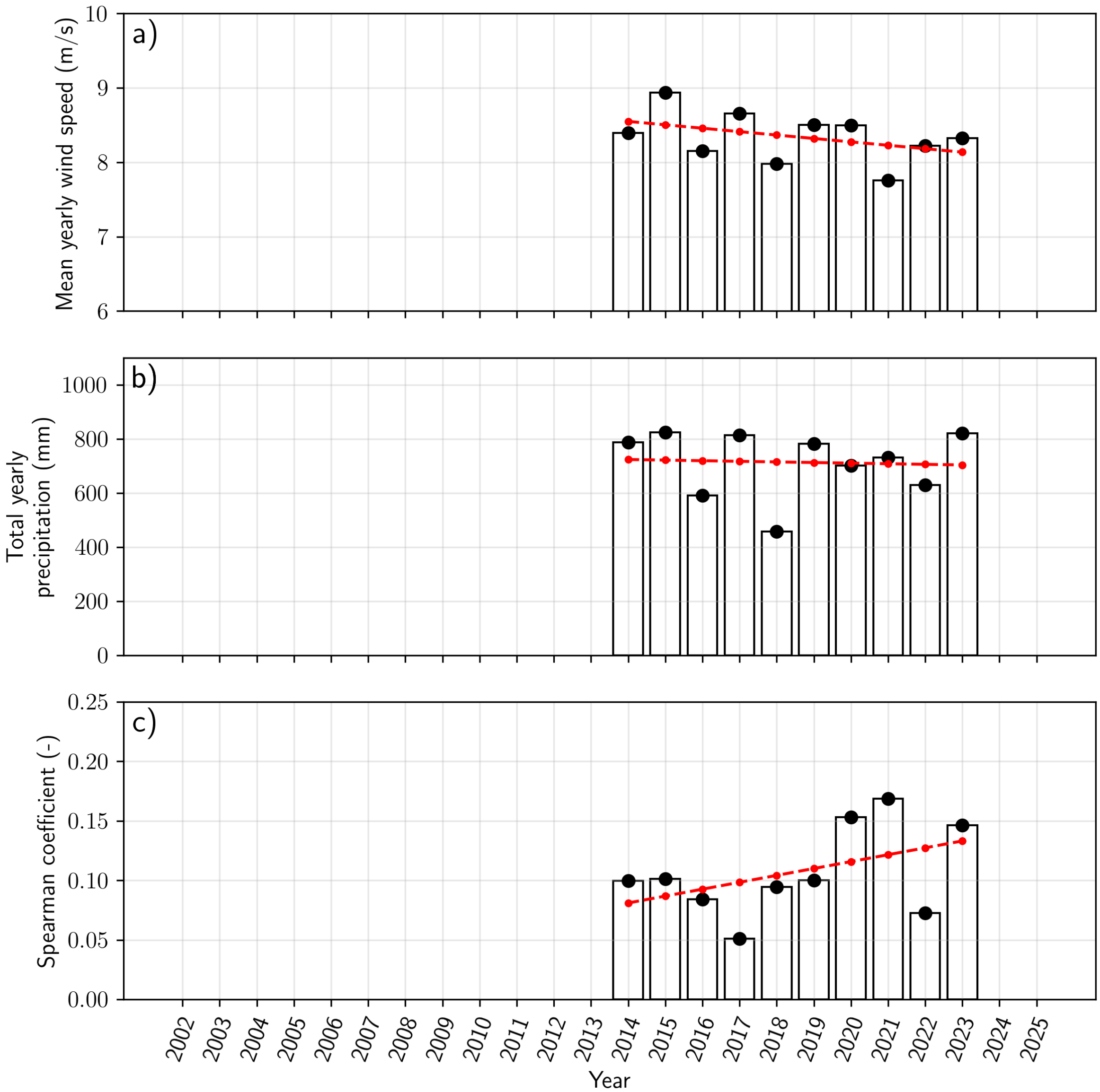

Figure 5. Mean yearly wind speed from NEWA at 150 m height, mean yearly precipitation from IMERG and Spearman coefficient for Risø, DTU.

https://doi.org/10.5194/wes-2026-136
Preprint. Discussion started: 7 August 2026
© Author(s) 2026. CC BY 4.0 License.

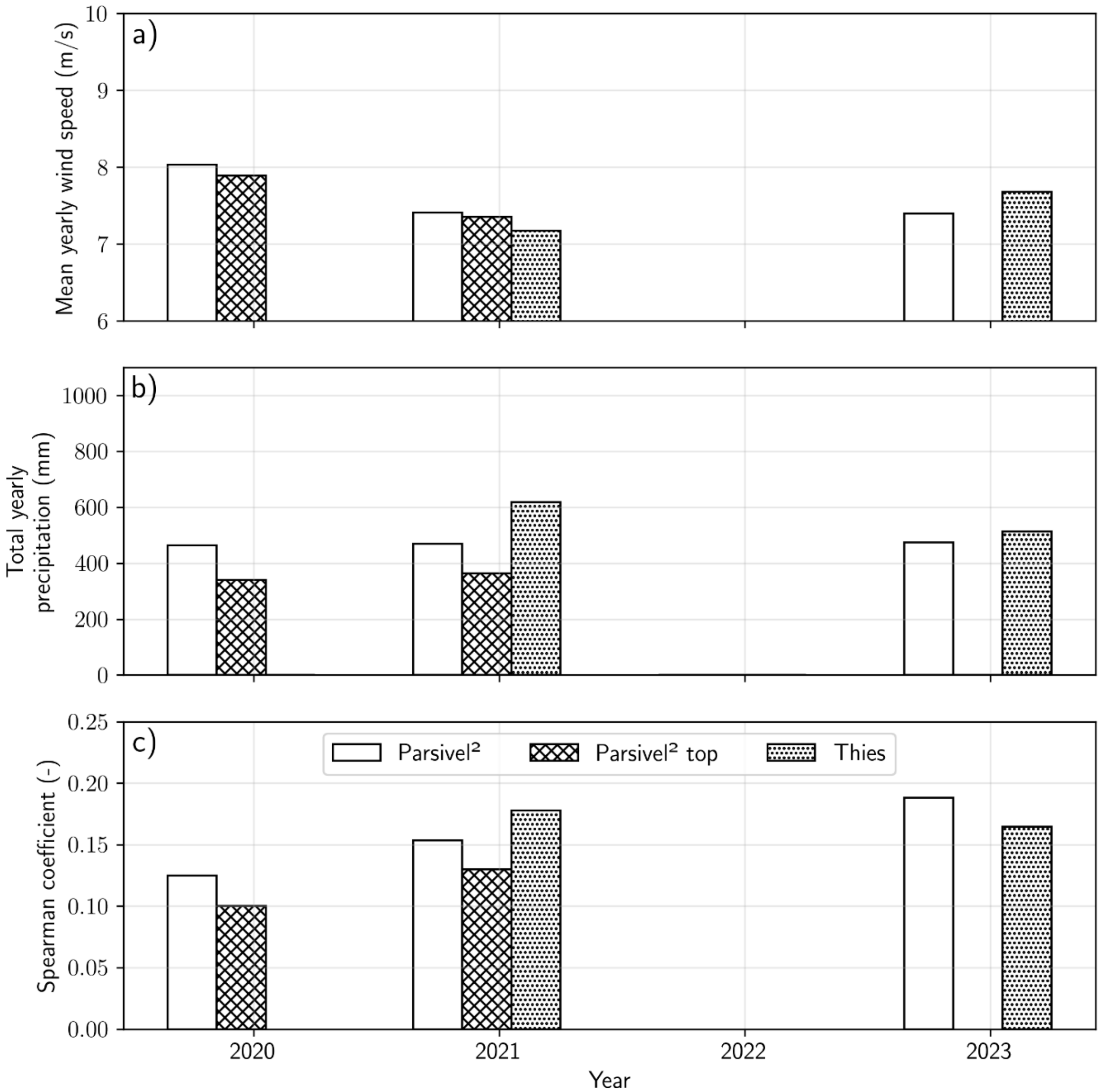

295 **Figure 6. Mean yearly wind speed from sonic at 60m height, mean yearly precipitation from Parsivel², Parsivel² top and Thies disdrometers, and Spearman coefficient for Risø, DTU.**

https://doi.org/10.5194/wes-2026-136
Preprint. Discussion started: 7 August 2026
© Author(s) 2026. CC BY 4.0 License.

4.2 End of Incubation (EoI)

EoI is assessed based on the assumption that three reference turbines were located at Risø during the weather conditions shown in Fig. 4. EoI assessment is based on a 19-year time series of rain gauge and cup anemometer observations at 10-minute temporal resolution.

Examining the impact on EoI for three reference turbines is based on the droplet slowdown impact efficiency, evaluated using two methods (DNV, 2021; Barfknecht and von Terzi, 2024). The latter is a more comprehensive method than recommended by DNV. Results are summarized in Table 3. Longer lifetimes (~24% increase) are observed with the advanced droplet slowdown model. The choice of droplet slowdown method adds uncertainty in EoI assessment.

The turbine type with higher maximum tip speed (IEA 15 MW) shows shorter EoI than turbines with lower maximum tip speeds. For NREL 5 MW, EoI is far beyond 25 years while for DTU 10 MW ~50% of 25 years. The IEA 15 MW turbine has an EoI far below 25 years and is thus the focus of our following assessment.

Table 3. End of incubation using two impact efficiency methods for three turbines based on 19 years of cup anemometer and rain gauge observations at Risø, DTU.

Impact efficiency method	DNV (2021)	Barfknecht and von Terzi (2024)
Turbine	End of incubation (years)	
NREL 5 MW	39.1	47.6
DTU 10 MW	12.5	15.6
IEA 15 MW	5.5	6.8

EoI results are presented for the IEA 15 MW turbine using the droplet slowdown method following Barfknecht and von Terzi (2024). The available weather data sources are used jointly with rain gauge and cup anemometer, disdrometer and sonic, and IMERG and NEWA. Note only the precipitation sources are mentioned in the following. Results from rain gauge show a decrease in EoI for 19 years (Fig. 7a) and from IMERG a decrease in EoI for 10 years (Fig. 7b). Results from disdrometer are shown in Fig. 7c.

The range of EoI values in Fig. 7 is summarized in Table 4, which shows the minimum, mean, median, and maximum EoI for each available data set. The variability in EoI between years and data sources is high. It is noted that the longer the time series, the larger the span from minimum to maximum EoI. Mean EoI is 7.5 years for rain gauge, 5.7 years for IMERG, 9.1 years for Parsivel^2, 12.8 years for Parsivel^2 top, and 7.1 years for Thies. The data source and length of the time series add uncertainty to the assessment of EoI.

https://doi.org/10.5194/wes-2026-136
Preprint. Discussion started: 7 August 2026
© Author(s) 2026. CC BY 4.0 License.

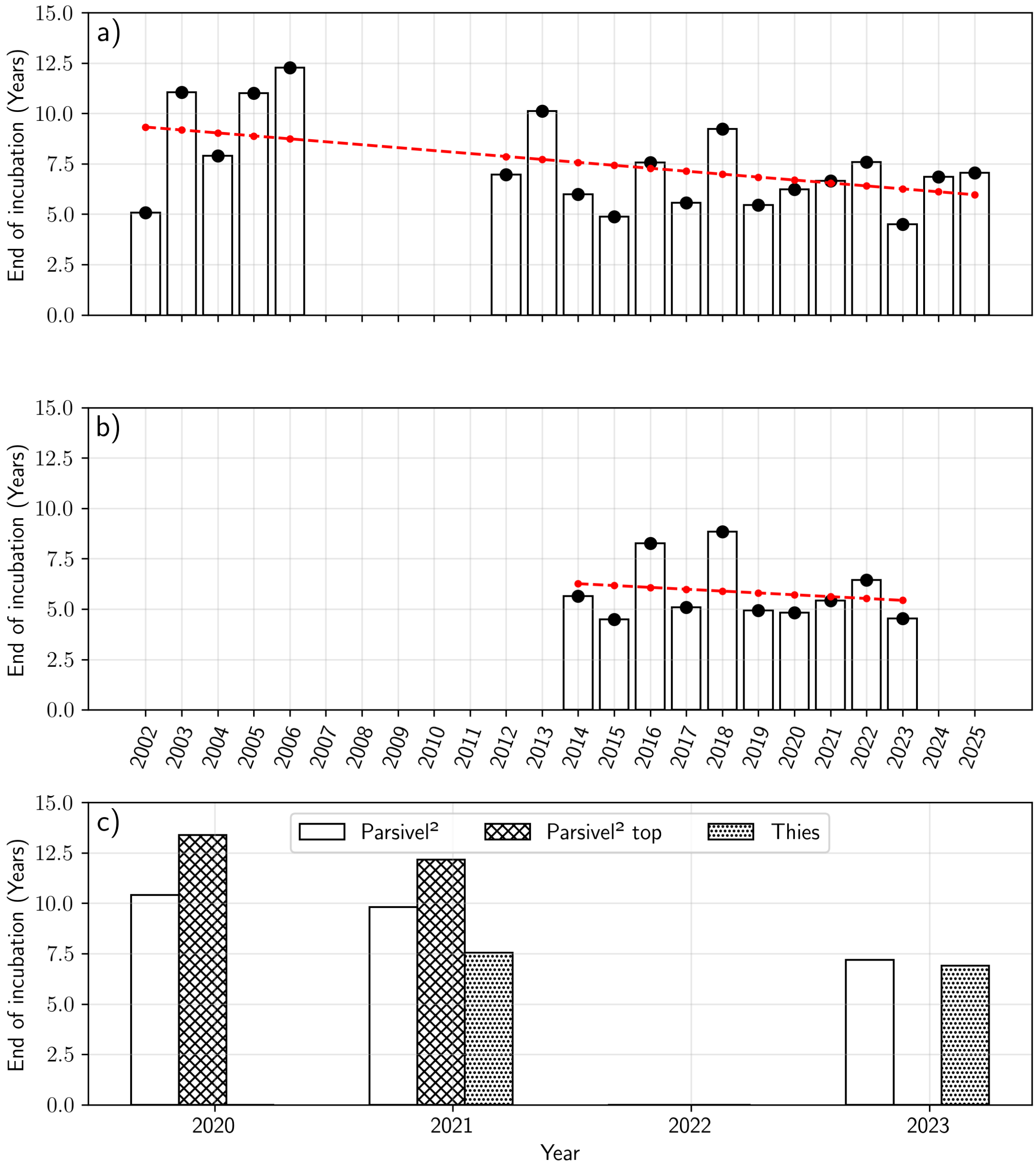

330 **Figure 7. End of incubation and trendline predicted for a 15 MW turbine based on a) cup anemometer and rain gauge, b) NEWA and IMERG, and c) sonic and three disdrometers observations at Risø, DTU.**

https://doi.org/10.5194/wes-2026-136
Preprint. Discussion started: 7 August 2026
© Author(s) 2026. CC BY 4.0 License.

Table 4. End of incubation for IEA 15 MW turbine based on weather data covering Risø, DTU.

Source	Period (years)	End of incubation (years)			
		Min	Median	Mean	Max
Rain gauge and cup anemometer	19	4.5	7.0	7.5	12.3
IMERG and NEWA	10	4.5	5.3	5.7	8.8
Parsivel^2 and sonic	3	7.2	9.8	9.1	10.4
Parsivel^2 top and sonic	2	12.2	12.8	12.8	13.4
Thies and sonic	2	6.9	7.2	7.19	7.6

Interannual variations in EoI persist across all data sources. This fact raises the question of uncertainty in the assessment of EoI using a short or long time series. The results from the sensitivity analysis on the uncertainty on the assessment of EoI related to using one 'representative' year versus longer consecutive time periods using the 19-year data source are shown in Fig. 8. The variability in EoI varies from 4.5 years to 12.3 years using only one year of data, ~170% differences. The span of years in the 25- to 75-percentiles is 5.8 to 8.6 years, a ~50% difference. For a 10-year time series, uncertainty is considerably reduced compared to a 1-year time series. The minimum and maximum range from 6.1 to 7.5 years (~23% difference), while the 25th and 75th percentiles are 6.4 and 7.2 years (12% difference). The median of EoI varies slightly across years, even for time series longer than 10 years.

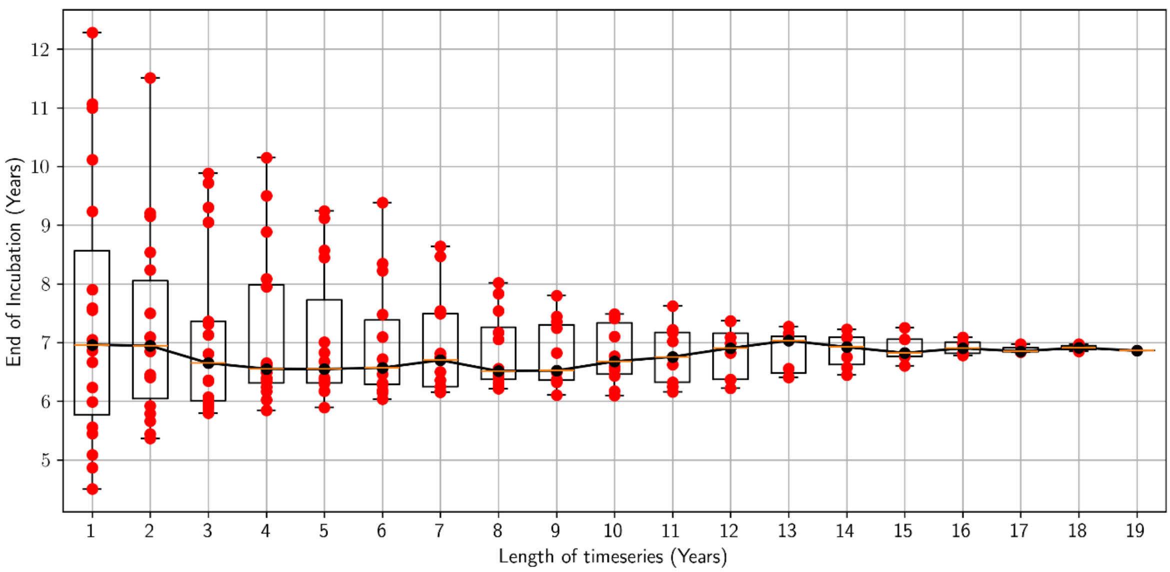

Figure 8. Sensitivity analysis on end of incubation using length of time series from 1 to 19 years for a 15 MW turbine, based on rain gauge and cup anemometer observations at Risø, DTU, of EoI median, minimum, maximum, 25th and 75th percentiles.

https://doi.org/10.5194/wes-2026-136
Preprint. Discussion started: 7 August 2026
© Author(s) 2026. CC BY 4.0 License.

Considering the effect of temporal resolution, data sources are resampled to a lower temporal resolution to compare EoI across lower-resolution data. In 2020, 2021, and 2023, three data sources (Parsivel^2, rain gauge, IMERG) are available, and the EoI results for 1-, 5-, 10-, 30-, and 60-minute are listed in Table 5. The results indicate decreasing EoI with lower temporal resolution for the disdrometer and a modest reduction for IMERG, while the rain gauge shows inconsistent results.
Results on EoI for one year, 2021, separating between five data sources (Parsivel^2, Parsivel^2 top, Thies, rain gauge, IMERG) are presented in Table 6. EoI decreases for lower temporal resolution for Parsivel^2, Parsivel^2 top and IMERG while Thies show an increase and rain gauge is inconsistent. EoI using resampled data shows variations from ~0 to 10%, but no systematic behavior. The under catch in disdrometers leads to longer EoI for all disdrometers compared to rain gauge and IMERG.

Table 5. End of incubation from 1-minute (Parsivel^2 and sonic), 10-minute (rain gauge and cup anemometer), 30-minute (IMERG and NEWA), and all observations resampled to lower temporal resolution for the period 2020, 2021, and 2023 at Risø, DTU.

Data source	End of incubation at different temporal resolutions (years)				
	1min	5 min	10 min	30 min	60 min
Parsivel^2 and sonic anemometer	8.4	7.8	7.7	7.7	7.7
Rain gauge and cup anemometer	NA	NA	5.4	5.3	5.4
IMERG and NEWA	NA	NA	NA	4.9	4.8

Table 6. End of incubation from 1-minute (disdrometers and sonic), 10-minute (rain gauge and cup anemometer), 30-minute (IMERG and NEWA), and all observations resampled to lower temporal resolution for the period 2021 at Risø, DTU.

Data source	End of incubation at different resolutions				
	1 min	5 min	10 min	30 min	60 min
Parsivel^2 and sonic anemometer	9.8	9.7	9.5	9.6	9.6
Parsivel^2 top and sonic anemometer	12.2	12.0	11.7	11.9	11.8
Thies and sonic anemometer	7.6	7.9	7.9	8.1	8.3
Rain gauge and cup anemometer	NA	NA	6.66	6.73	6.63
IMERG and NEWA	NA	NA	NA	5.42	5.27

4.3 Erosion safe operation efficiency (Pareto front)

https://doi.org/10.5194/wes-2026-136
Preprint. Discussion started: 7 August 2026
© Author(s) 2026. CC BY 4.0 License.

The relevance of applying ESO for a given turbine at a specific site depends upon a range of parameters. Preferably, a multi-year time series on precipitation and wind speed is acquired to assess the overall potential.

Firstly, ESO efficiency is assessed similarly to the initial assessment of EoI, using three reference turbines based on a 19-year time series of rain gauge and cup anemometer observations at a 10-minute temporal resolution, and accounting for the impact of two droplet slowdown methods (DNV, 2021; Barfknecht and von Terzi, 2024). ESO efficiency is shown in Fig. 9.

For an AEP loss of 0% corresponding to normal operation, i.e., without a curtailment strategy to extend blade lifetime, the EoI values in Fig. 9 and Table 3 correspond. If the turbines are operated such that AEP is reduced by 0.4% during the most damaging 10-minute periods, the EoI for the NREL 5 MW is extended to ~150 and ~170 years, for methods based on DNV (2021) and Barfknecht and von Terzi (2024), respectively. The advanced droplet slowdown model shows a flatter curve than the DNV method. The flatter Pareto front corresponds to higher ESO efficiency, i.e., the damage is reduced for a relatively lower AEP loss. Applying the droplet slowdown model (Barfknecht and von Terzi, 2024) increases the benefit of ESO compared to the DNV method (DNV, 2021). The advanced droplet-impact efficiency is expected to represent damage progression better than the DNV method. The steeper Pareto front for the IEA 15 MW turbine than for the other two turbines shows that a large AEP loss is needed to reduce damage.

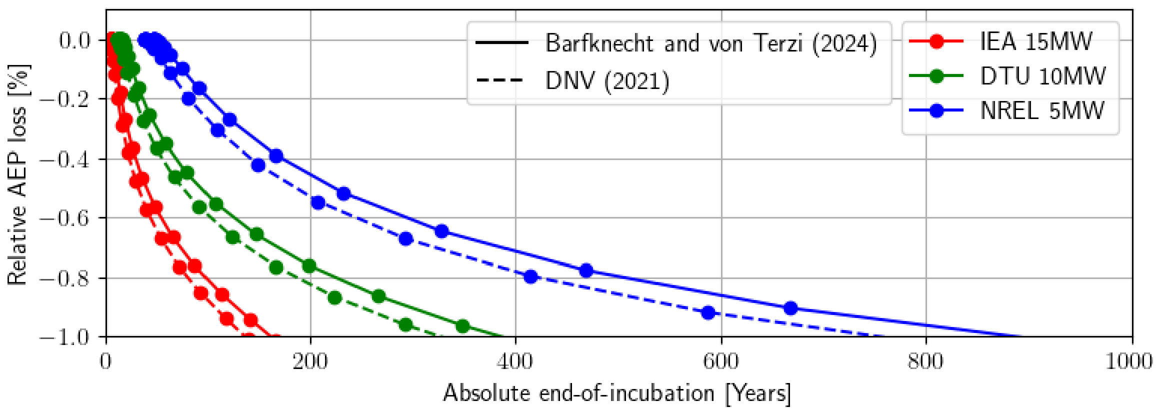

Figure 9. Erosion safe operation efficiency Pareto front showing relative AEP loss and absolute EoI for three reference turbines for the DNV and droplet slowdown methods based on 19 years of rain gauge and cup anemometer observations at Risø, DTU.

Next, ESO efficiency uncertainty is examined further for an IEA 15 MW turbine, and the advanced droplet slowdown method is selected (in all subsequent assessments). Results from a 19-year series are used and plotted in Fig. 10. In contrast to Fig. 9, not only is EoI given, but also the uncertainty from Monte Carlo simulations, yielding a range of Pareto fronts. The Pareto front in Fig. 9 for the IEA 15 MW turbine using the advanced droplet slowdown does not exactly match the EoI values in Fig.

https://doi.org/10.5194/wes-2026-136
Preprint. Discussion started: 7 August 2026
© Author(s) 2026. CC BY 4.0 License.

10 due to the probabilistic method. The probabilistic method samples equal to one year of weather data (Fig. 10) while the time series method uses all 19 years of samples (Fig. 9).

In Fig. 10, the distributions broaden with increasing AEP loss. The weather distribution is narrower than the material distribution. The results of minimum, median, mean, and maximum EoI for AEP loss of 0.2% are listed in Table 7. The total uncertainty in EoI, summing the contributions from weather and materials, yields a median EoI of 9.9 years. Median EoI is smaller than mean EoI (10.2 years), due to a skewed distribution with maximum EoI (~ 20 years) and minimum EoI (~ 4 years). Interestingly, the uncertainty due to weather ranges from ~8 to ~10 years, while the uncertainty due to material ranges from ~4 to 20 years.

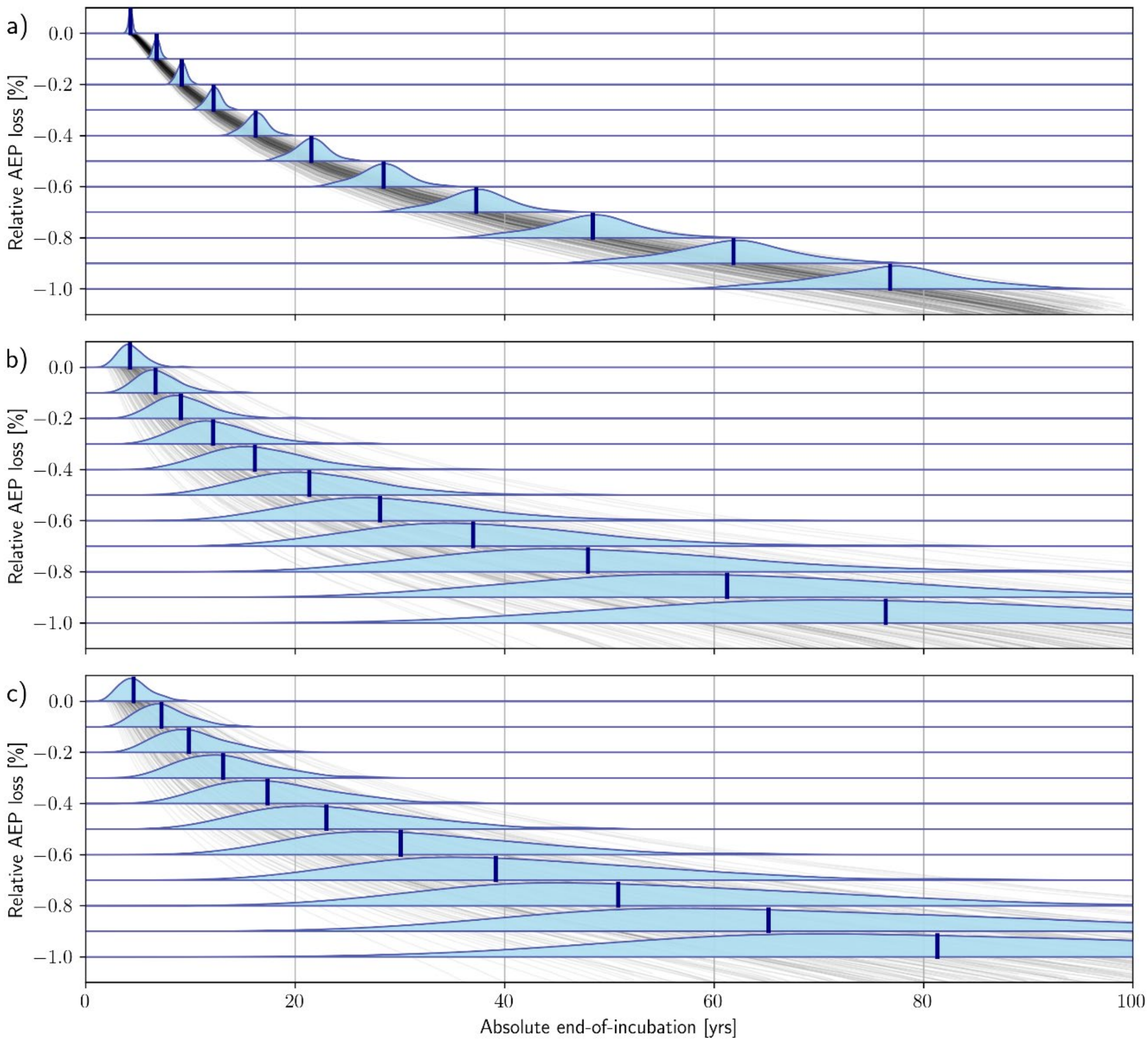

Figure 10. Erosion safe operation efficiency Pareto fronts uncertainty for a) weather, b) material, and c) total combined, for IEA 15 MW turbine based on rain gauge and cup anemometer observations for 19 years at Risø, DTU.

https://doi.org/10.5194/wes-2026-136
Preprint. Discussion started: 7 August 2026
© Author(s) 2026. CC BY 4.0 License.

Table 7. Erosion safe operation efficiency listing end of incubation uncertainty in the form of minimum, median, mean, and maximum for weather, material, and total combined, for IEA 15 MW turbine based on rain gauge and cup anemometer observations for normal operation (AEP loss 0%) and curtailment (AEP loss 0.2%) at Risø, DTU.

Causes	AEP loss	End of incubation (years)			
	(%)	Min	Median	Mean	Max
Weather	0	3.8	4.2	4.3	4.8
	0.2	8.0	9.2	9.2	10.4
Material	0	1.9	4.2	4.4	9.3
	0.2	4.1	9.1	9.4	20.2
Total	0	1.9	4.7	4.7	9.4
	0.2	4.1	9.9	10.2	20.4

ESO efficiency Pareto fronts are shown for three years (2020, 2021, and 2023) based on Parsivel^2, rain gauge, and IMERG in Fig. 11. The positive bias of EoI based on Parsivel^2 due to ~25% missing data is noted. For an AEP loss of 0% Parsivel^2 shows EoI 8.4 years, the rain gauge 5.4 years, and IMERG 4.9 years in Fig. 11 (values are listed in Table 6).

The steepest Pareto front is found for the lowest temporal resolution data (IMERG), and the flattest Pareto front for the highest temporal resolution data (Parsivel^2) (Fig. 11). The steepness is expected to increase with lower temporal resolution, as the short-lived, highly damaging events are less accurately observed in lower temporal resolution observations. The Pareto front based on the rain gauge lies between the two others at AEP loss 0 to 0.6% but has a much flatter curve than the Parsivel^2. The flatter curve is unexpected. The Pareto front curve intersects the Parsivel^2 Pareto front at AEP loss 0.6%. The flatness and intersection may be explained by the resolution of observations from rain gauge 1.2 mm h^{-1}, which is more than a factor of 10 lower than those from the Parsivel^2 and IMERG (0.1 mm h^{-1}). The rain gauge overestimates ESO efficiency because it misses observations below 0.2 mm per 10 min, as the tip only triggers when this amount of water is collected. In contrast, the Parsivel^2 and IMERG have finer measurement resolution.

To assess the sensitivity of ESO efficiency to temporal-resolution resampling, data are resampled. The Parsivel^2 and sonic time series at 1-minute frequency are resampled to 10- and 30-minute values for three years (2020, 2021, and 2023). The rain gauge and cup anemometer time series at 10-minute frequency are resampled to 30-minute values. The EoI results for the original and resampled time series are shown in Fig. 11. ESO efficiency decreases with lower temporal resolution, as expected. ESO efficiency results based upon resampled Parsivel^2 data approach the steepness of IMERG Pareto front, though the latter is slightly steeper. ESO efficiency results based on resampled rain gauge data show flatter curves than resampled Parsivel^2 data. The flatter curve based on the rain gauge is probably due to the rain gauge's lower measurement resolution compared to the Parsivel^2 and IMERG.

https://doi.org/10.5194/wes-2026-136
Preprint. Discussion started: 7 August 2026
© Author(s) 2026. CC BY 4.0 License.
Open Access WIND ENERGY SCIENCE DISCUSSIONS

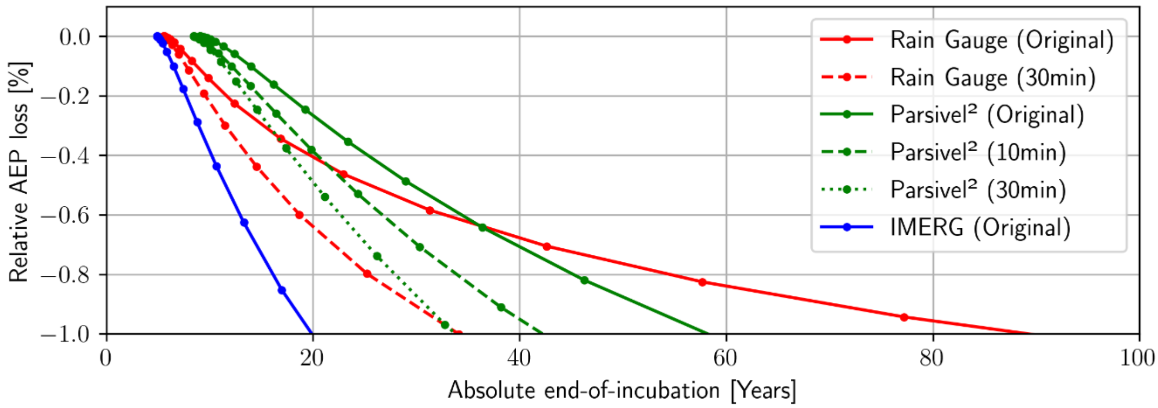

Figure 11. Erosion safe operation efficiency Pareto fronts showing relative AEP loss and absolute end of incubation for IEA 15 MW turbine based on rain gauge and cup anemometer, Parsivel^2 and sonic, and IMERG and NEWA original and resampled observations for three years at Risø, DTU.

The total uncertainties for the three types of observations, calculated using Monte Carlo simulation, are shown in Fig. 12 and Table 8. Fig. 12 shows a larger spread in EoI based on the Parsivel^2 than on the rain gauge, and the smallest spread in EoI for IMERG at AEP loss 0%. However, for AEP losses larger than ~0.6%, the spread in EoI for the rain gauge is greater than that for the Parsivel^2. Rain gauge data overestimates ESO efficiency. The rain gauge result is not trustworthy because the rain gauge does not capture all details.

In contrast, IMERG underestimates ESO efficiency due to its lower temporal resolution relative to the Parsivel^2. The results in Table 8 show that for an AEP loss of 0%, median EoI values are consistently lower than the mean EoI across all data types, and the difference between the minimum and maximum is largest for the Parsivel^2, smallest for IMERG, and intermediate for the rain gauge. The difference between the minimum and maximum EoI for AEP loss 0.4% is larger for the rain gauge than the Parsivel^2 and IMERG and grows rapidly for larger AEP loss (Fig. 12).

The challenges in assessing ESO efficiency depend on accurately characterizing the joint distribution of precipitation and wind. The Parsivel^2 performs better than the rain gauge and IMERG to observe short-lived precipitation. However, for reliable assessment of EoI, under-catch and missing data pose a problem. For the assessment of ESO efficiency, under catch and missing data pose less of a problem, while the advantages of temporal resolution and high measurement resolution are important.

https://doi.org/10.5194/wes-2026-136
Preprint. Discussion started: 7 August 2026
© Author(s) 2026. CC BY 4.0 License.

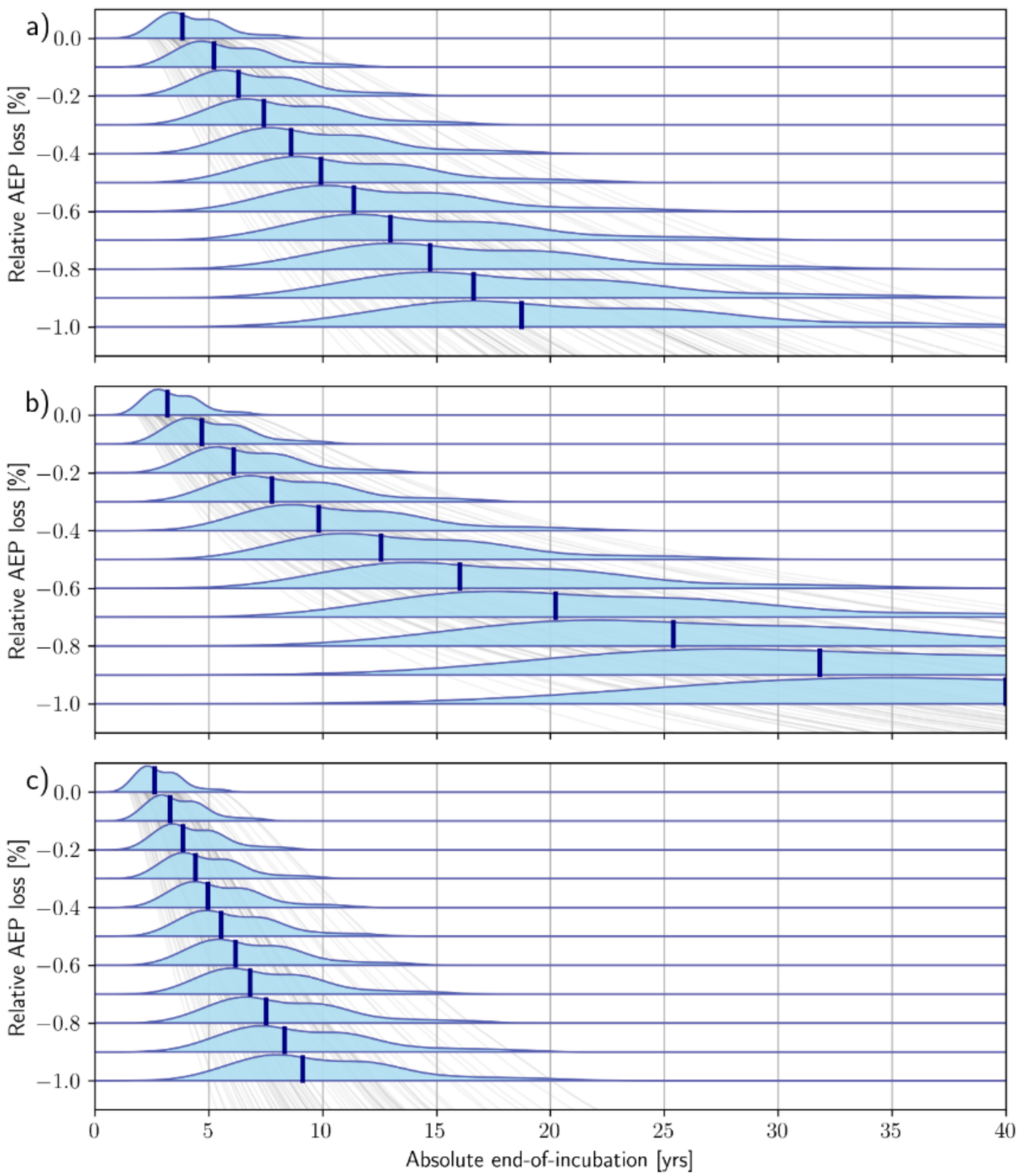

445

Figure 12. Erosion safe operation efficiency Pareto fronts showing total uncertainty for IEA 15 MW turbine based on a) Parsivel² and sonic, b) rain gauge and cup anemometer, c) IMERG and NEWA for three years at Risø, DTU.

https://doi.org/10.5194/wes-2026-136
Preprint. Discussion started: 7 August 2026
© Author(s) 2026. CC BY 4.0 License.

Table 8. Erosion safe operation efficiency listing end of incubation uncertainty in the form of minimum, median, mean, and maximum for IEA 15 MW turbine on Parsivel² and sonic, rain gauge and cup anemometer, and IMERG and NEWA for normal operation (AEP loss 0%) and curtailment (AEP losses of 0.2% and 0.4%) at Risø, DTU.

Sources	AEP loss (%)	End of incubation (years)			
		Min	Median	Mean	Max
Parsivel² and sonic	0	2.2	3.8	4.3	8.2
	0.2	3.6	6.3	7.1	13.8
	0.4	4.9	8.6	9.7	18.9
Rain gauge and cup anemometer	0	1.8	3.2	3.5	6.7
	0.2	3.3	6.1	6.7	13.0
	0.4	5.2	9.8	10.8	21.2
IMERG and NEWA	0	1.5	2.6	2.9	5.6
	0.2	2.2	3.9	4.3	8.4
	0.4	2.7	5.0	5.5	10.8

The ESO efficiency uncertainty, based on three disdrometers observed over one year (2021), is presented in Fig. 13. The total uncertainty is lowest under normal operating conditions and increases with increasing AEP loss. For normal operation with AEP loss 0%, EoI for Parsivel² is 9.8 years, Parsivel² top 12.2 years, and Thies 7.6 years (Fig. 13 and Fig. 7c). Parsivel² and Thies show curves of similar steepness and spread in Pareto fronts. In contrast, the Parsivel² top shows a flatter Pareto front and greater uncertainty than the two ground-based disdrometers (Fig. 13).

https://doi.org/10.5194/wes-2026-136
Preprint. Discussion started: 7 August 2026
© Author(s) 2026. CC BY 4.0 License.

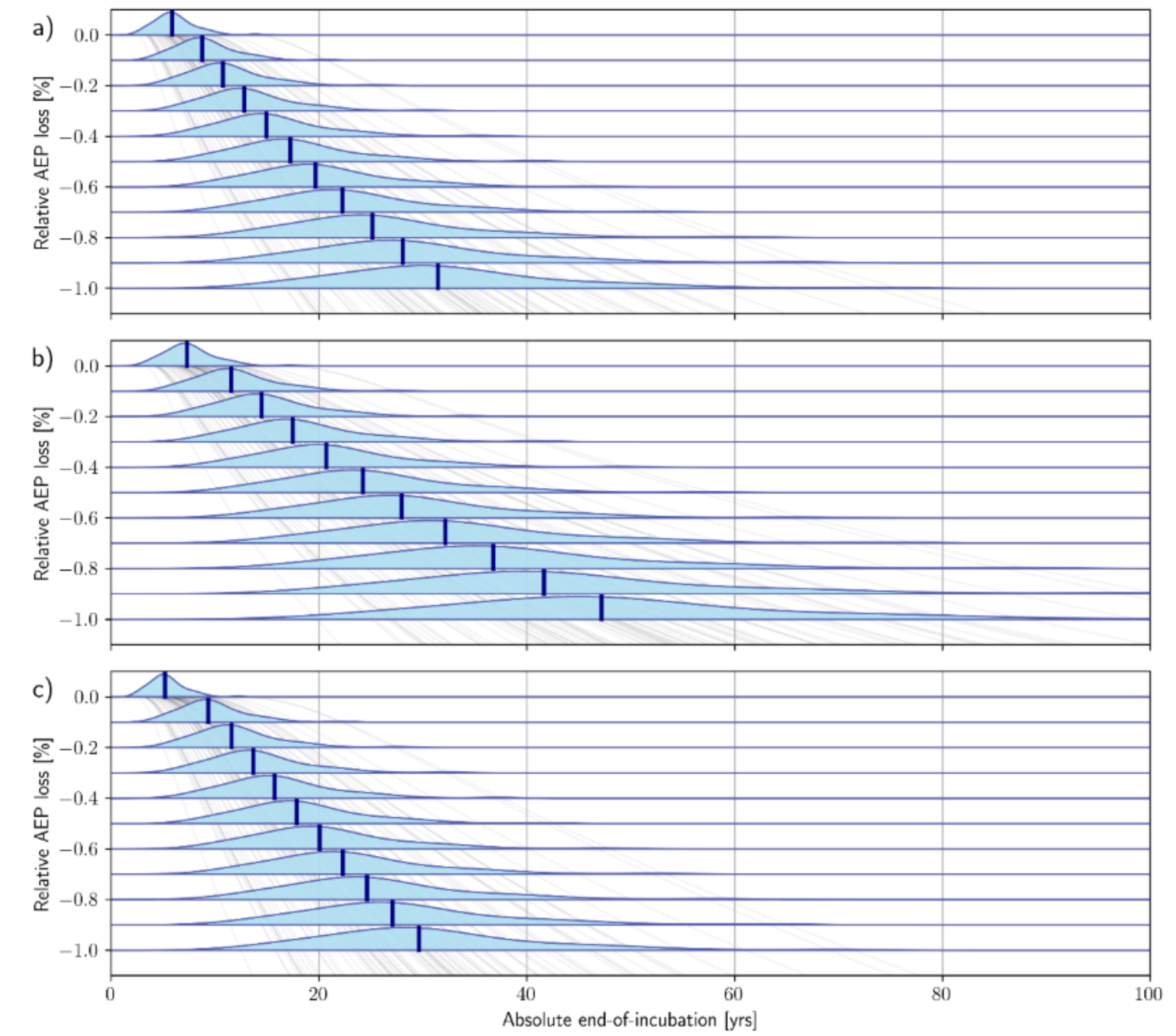

Figure 13. Erosion safe operation efficiency Pareto fronts showing end of incubation total uncertainty for IEA 15 MW turbine based
465 **on disdrometer and sonic for a) Parsivel², b) Parsivel² top, c) Thies observations for one year at Risø, DTU.**

5 Discussion

5.1 Weather conditions

The study is based on observations of precipitation rate, i.e., the sum of liquid and solid precipitation. Disdrometer and IMERG observations separate liquid and solid precipitation types. For IMERG, it is the likelihood for liquid and solid precipitation (Xiong et al., 2022). The rain gauge provides only the precipitation rate, and for consistency, the precipitation rate is selected from the disdrometer and IMERG in the current study. The amount of solid precipitation in Denmark is low. Results based on IMERG for Risø shows 97.8% liquid and 2.2% solid precipitation for 10 years. Most of the solid precipitation in Denmark is snowfall. In other climates, solid precipitation is frequent, with implications for the assessment of EoI, e.g., Navarra, Spain (Dimitriadou and Hasager, 2026) and hail in the US (Pryor and Barthelmie, 2026). In case of hail, LEE is severe compared to rain droplets of similar diameter. This study focuses on uncertainties in EoI and ESO efficiency while ignoring the potential effect of hail on LEE at the Risø site.

The variability in collocated data of two long-tailed distributions, the Weibull distribution of wind speeds and the Gamma distribution of precipitation rates, requires many years of observations to characterize the joint distribution for the high-end tail of both parameters. Heavy precipitation during high-wind events causes significant damage. In the current study, the joint distribution varies from year to year, quantified by the Spearman coefficient. The Spearman coefficient is consistently positive across all data sources and years and shows an increasing trend in the data sets spanning 10 and 19 years. The increase in the Spearman coefficient in later years is driven by rising precipitation at the Risø site, which aligns well with climate trends in Denmark, showing an increase in annual average precipitation during recent decades (DMI, 2025).

Advantages of rain gauge observations are long series, ≥25 years (Nash et al., 2021; Verma et al., 2021a; Verma et al., 2021b) and limited data loss. In our case, missing data is ~5% for 19 years. Limitations of rain gauge observations are a low measurement resolution (1.2 mm h^{-1}) in the current data set and without classification of liquid and solid precipitation. Rain, snow and hail impact blades differently though not considered in the current study.

In contrast to rain gauge, disdrometer are short series and suffer from missing data. In our study ~25% missing data and under-catching precipitation. The Parsivel^2 at the ground at a sheltered location and Parsivel^2 top at a windy location show the latter to observe less precipitation (resulting in longer EoI). A study in the Netherlands showed disdrometer data to suffer from under catch and missing data (Caboni et al., 2024). Advantages of disdrometer are high temporal resolution (1 minute) and high measurement resolution (0.1 mm h^{-1}). Additionally, precipitation types and droplet size distribution (DSD) are recorded by disdrometer though not used in the current study.

Research on EoI using DSD at offshore, coastal, and inland stations in the Netherlands show that many small droplets are observed. However, droplets with diameters smaller than 0.8 mm contribute very little to erosion progression compared with larger droplets (Caboni et al., 2024). Caboni et al. (2024) conclude that DSD is secondary for the assessment of EoI and suggest rain gauge and radar measurements. Campobasso et al. (2026) report that EoI, identified with rain rate and calculated mass-weighted droplet diameter based on Best (1950), correlates better with rain rate than the disdrometer-measured DSD mass-weighted diameter.

An assessment of EoI using three types of disdrometers in the US showed variation in EoI from 15 to 27 years (Letson and Pryor, 2023), based on the Springer damage model (Springer, 1976) and droplet-size distribution, counting the number of droplets (Marshall and Palmer, 1948). According to Castorrini et al. (2024), EoI using the Springer model showed shorter lifetimes than rain-erosion test-based damage models, and the latter performed better compared to damage observed in turbine blades operating in the UK, based on disdrometer and rain-gauge data. Sánchez et al. (2026) compared the Springer model and

https://doi.org/10.5194/wes-2026-136
Preprint. Discussion started: 7 August 2026
© Author(s) 2026. CC BY 4.0 License.

the rain erosion test-based damage model for a wind farm in Denmark and found the latter to better correspond to the damage observed in the field. Hannesdóttir et al. (2024b) tested EoI sensitivity to DSD and function from Best (1950) and found variations in EoI using an impingement model. In summary, research indicates DSD does not per se improve assessment of EoI compared to using rain rate and a model function for DSD. Noting that the Springer model uses the number of impacts, it may be preferable to ensure an accurate number of droplets. In contrast, the impingement model uses the volume of water; it may be preferable to ensure an accurate amount of water when selecting the DSD model function.

Advantages of IMERG observations are long time series, high measurement resolution (0.1 mm h^{-1}), classification of liquid and solid precipitation based on a likelihood estimator, and limited missing data, in our case ~0%, but missing data (or low data quality) varies by location. The key difference between IMERG and local observations is the spatial extent, covering 11 km grid cells, and precipitation variations within a grid cell. Limitations of IMERG are temporal resolution of 30 minutes not capturing short lived peaks, e.g., during convective precipitation fully. The accuracy of IMERG within Europe was assessed by researchers and found to outperform numerical model (Retalis et al., 2022; Ivanova, 2025). IMERG has been used for EoI assessment with good results compared to local observations (Badger et al., 2022; Dimitriadou et al., 2024; Dimitriadou and Hasager, 2026).

Wind speed observations from cup anemometer, sonic and NEWA are selected for good quality data and with few missing data for cup anemometer and sonic. For NEWA model results no missing values but general uncertainty on model results would exist. Risø is a flat location presumably with winds modelled well. It is considered beyond scope in the current study to investigate wind speeds in detail. Appendix A includes an example on vertical extrapolation of wind speed observed at the meteorological mast and the effect on EoI and ESO Pareto fronts.

5.2 Uncertainties for assessment of the end of incubation

A major source of uncertainty in the assessment of EoI is the length of the time series. The uncertainty in EoI when using one year out of 19 years results in ~170% differences between the shortest and longest EoI (4.5 years to 12.3 years) for the IEA 15 MW turbine example at the Risø site. For a 10-year time series, there is a ~23% difference between the minimum and maximum EoI and a ~12% difference in EoI in the 25- to 75-percentile range. The result on uncertainty in EoI is comparable to findings for three sites in the US, varying the time series length from 1 to 17 years (Pryor et al., 2025), and for sites in Northern Europe, varying the time series length from 1 to 16 years (Hasager et al., 2021). Pryor et al. (2025) identified more than 100% variation between the minimum and maximum EoI for assessments based on one- and two-year periods compared to the long-term EoI value. Bartolomé and Teuwen (2021) found that annual values of erosive variables exhibited high standard deviations from one year to the next, based on 25 years of data in the Netherlands. Caboni et al. (2024) suggest using longer-term rain-gauge and radar measurements for EoI assessment rather than short-term data from disdrometers.

https://doi.org/10.5194/wes-2026-136
Preprint. Discussion started: 7 August 2026
© Author(s) 2026. CC BY 4.0 License.

In case a 'representative' year or short period needs to be selected to assess EoI, it is suggested to assess the EoI from a long time series and next identify a 'representative' period aligning with the mean or median EoI to ensure the joint wind and precipitation distribution represents the longer-term joint distribution.

Assuming constant weather conditions as in the DNV RP versus time-series synchronized distribution has been found to causes 70% overestimation of EoI at a site in the UK (Castorrini et al., 2024), 90% overestimation in the UK (Visbech et al., 2025), and above 200% overestimation at two sites in the UK (Simon et al., 2026).

Another large uncertainty for assessment of EoI stems from the droplet impact efficiency model used. Based on the DNV RP method, EoI is 5.5 years, while the comprehensive method by Barfknecht and von Terzi (2024) yields EoI of 6.8 years for the IEA 15 MW turbine, using 19 years of observations. The difference is ~24%. Castorrini et al. 2024 identified up to a 12% longer EoI period, including aerodynamic effects on droplet impingement, thereby enabling an assessment of smaller droplets being deflected from the airfoil at a site in the UK.

Comparing EoI from rain gauge and IMERG for a 10-year concurrent period shows rain gauges at ~7 years and IMERG at ~5 years (difference ~30%). IMERG shows slightly less precipitation than rain gauge observations. The difference may be due to either higher co-variations in precipitation and wind speeds for IMERG (Spearman coefficient ~0.1) than rain gauge (~0.05), or 150 m NEWA wind speeds higher than wind speeds extrapolated to 150 m from 10-minute wind speeds observed at 125 m (not tested), or a combination. IMERG has much better measurement resolution than rain gauge, however, IMERG covers an area while the rain gauge is local point.

EoI assessed based on two similar disdrometers, one mounted at ground level (Parsivel^2) and one at a height of 123 m (Parsivel^2 top) shows, respectively, ~10 years and ~12 years (~20% difference). At the top, wind-induced drop diversion might occur to a greater degree than at the base, causing under catch, hence longer EoI. There might also be variability in the DSD at the two heights, e.g., DSD with smaller droplets at higher height than observed at the ground

EoI assessed based on two types of disdrometers mounted at ground level (Parsivel^2 and Thies), shows, respectively, ~10 years and ~8 years (~20% difference). Thies has more missing data than Parsivel^2. However, Thies measured more precipitation and showed higher Spearman coefficient than Parsivel^2, suggesting Thies observed more precipitation during windy conditions than Parsivel^2. This may explain the shorter EoI based on Thies.

Monte Carlo simulations provide uncertainty estimates for EoI depending on weather, materials, and the combined effect. Interestingly, uncertainty due to weather was lower than that for the material at the investigated site. The results on variability in EoI explain the otherwise counterintuitive fact that the erosion levels among three blades of a turbine may differ.

In summary, EoI assessment is recommended to be based on a long time series with few missing data.

5.3 Uncertainties in assessment of erosion safe operation efficiency

https://doi.org/10.5194/wes-2026-136
Preprint. Discussion started: 7 August 2026
© Author(s) 2026. CC BY 4.0 License.

A long series of precipitation and wind speed is needed to assess EoI, hence the overall relevance of ESO. Observations at the Risø site indicate EoI for the NREL 5 MW turbine is ~48 years, for the DTU 10 MW turbine is ~16 years, and for the IEA 15 MW turbine is ~7 years. ESO would not make sense for NREL 5 MW with EoI far beyond 25 years.

EoI is used as a proxy for the decision on curtailment and assessment of ESO efficiency. EoI is a very mild form of damage in which repair is not relevant, but aerodynamic performance degrades (Maniaci et al., 2025; Forsting et al., 2026). Erosion damage beyond EoI is relevant for the decision on repair (Mishnaevsky, 2019; Visbech et al., 2023). Rain erosion testing reports EoI but not damage levels beyond. The IEA 15 MW turbine has an EoI far below 25 years and is thus the focus of our investigation on ESO efficiency.

The modeling presented herein is based on a clean power curve, i.e., no change in power curve due to erosion. AEP loss due to rough blades could be refined, e.g., as in Campobasso et al. (2026), using a moderate- and severe-leading-edge-erosion state of the power curve. The effect of using power curves for eroded blades is most pronounced at low wind speeds, leading to relatively higher AEP losses.

The temporal resolution of meteorological data profoundly influences the assessment of ESO efficiency. The steepness of the Pareto front varies greatly across 1- to 30-minute temporal resolutions (Fig. 12). Resampling Parsivel^2 data to 30-minute values yields Pareto front steepness like IMERG, as expected. A study on ESO efficiency across different temporal resolutions found that the effectiveness of ESO increases with higher frequency, especially for sites with rapid variations in rainfall rate (Campobasso et al., 2026). Letson and Pryor (2023) investigated the percentage of curtailment time and the extended EoI period at 1- and 10-minute intervals and found that a few hours per year are cost-effective in the US. Letson and Pryor (2023) conclude that high temporal resolution is needed, as many severe events are short-lived. A newly established database linking disdrometer observations from all continents could be valuable for assessing ESO efficiency across various climates (Ghiggi et al., 2026).

The steepness of the ESO efficiency Pareto front based on rain gauge data starts between the disdrometer and IMERG from 0 to 0.2% AEP loss but then flattens and intersects the disdrometer Pareto front. Averaging rain gauge data to 30 minutes yields a steeper curve; however, it is flatter than the other 30-minute curves. The behavior of the Pareto front based on the rain gauge time series, which does not follow the other two Pareto fronts' curves, is likely due to the very different measurement resolution. Disdrometer and IMERG measure precipitation rate with a resolution of 0.1 mm h^{-1}, while the rain gauge resolution is 1.2 mm h^{-1} — a difference of more than one order of magnitude in measurement resolution between data types. The low measurement resolution of the rain gauge biases the Pareto front toward a too flat curve, i.e., overly optimistic values. It is concluded that disdrometer data are needed to assess ESO efficiency, whereas long-term data (e.g., rain gauges or IMERG) are needed to assess EoI.

Sites with few, short-lived, highly erosive weather events are more favorable for ESO than sites characterized by many long-lived, erosive weather events, resulting in small damage increments (Hasager et al., 2021; Pryor et al., 2025).

The meteorological variables of interest for ESO are, first, a long-term data set demonstrating the relevance of ESO, and second, high-frequency data with sufficient measurement resolution to assess ESO efficiency.

https://doi.org/10.5194/wes-2026-136
Preprint. Discussion started: 7 August 2026
© Author(s) 2026. CC BY 4.0 License.

Uncertainties due to probabilistic variability in weather, material, and combined uncertainty are quantified for a 19-year time series from the rain gauge and show larger uncertainty due to material than weather (Fig. 10). In case a decision is taken that 50% of blades in a wind farm should have EoI longer than ~10 years, an AEP loss of 0.2% would be needed. Some blades would have EoI ~4 years, and others EoI ~20 years (Table 7). As mentioned above, rain-gauge-based ESO efficiency is likely to overestimate the actual efficiency. Comparing ESO efficiency using the disdrometer, rain gauge, and IMERG over three years indicates that the rain gauge yields overly optimistic results; for example, for a 0.4% AEP loss, the disdrometer shows a median EoI of 8.6 years, while the rain gauge shows 9.8 years. IMERG shows 5.0 years. IMERG corresponds to a steeper Pareto front that underestimates ESO efficiency in case short-lived events with high damage increments prevail. Based on the disdrometer results, it is concluded that disdrometer data are needed at the Risø site to characterize the joint distribution of wind and precipitation and assess ESO efficiency.

Examining ESO efficiency across three disdrometers reveals substantial variation among them. Parsivel^2 and Thies show Pareto front curves with similar steepness and variability, while Parsivel^2 top shows flatter Pareto fronts and larger variability between minimum and maximum EoI.

It is relevant to account for droplet slowdown when assessing ESO efficiency. The advanced droplet slowdown model (Barfknecht and von Terzi, 2024) provides flatter curves than the DNV RP method.

The cost-effectiveness of ESO depends on electricity prices (Letson and Pryor, 2023; Skrzypiński et al., 2020). Bechmann and Quick (2025) showed that spot price data from the Nord Pool power exchange are negatively correlated with wind speed data at a site in Eastern Denmark. Risø is in the Nord Pool area. Between 2000 and 2023, the spot price decreased as wind speed increased. In contrast, the spot price increased for lower wind speeds in the same period. The high penetration of wind energy in Denmark causes a negative correlation between production prices and price volatility. It is necessary to balance the loss of income due to ESO-caused AEP loss against expenses related to blade repair and inspection downtime, AEP loss from operating turbines with eroded blades, as well as

the cost of precipitation sensors that provide reliable meteorological observations for the ESO strategy.

Hail is not investigated in the current study. In the US, Pryor and Barthelmie (2026) provide maps of days with hail on the US mainland based on radar data, showing that turbines in the Southern Great Plains could apply an ESO of ~80 hours, extending the EoI from 9.8 years to 14.8 years. The curtailment would be for the most erosive rain and hail events, with hail contributing between 25% and 38% of the accumulated damage. In some regions of Europe, hail prevails, according to Punge and Kunz (2016), and further investigation is relevant to assess EoI and ESO efficiencies for rain and hail contributions.

Studies in other climates, further analysis of meteorological data quality, the importance of hail, examination of VN curves, and inclusion of damage progression beyond EoI would be relevant future fields of investigation. Furthermore, the economic aspects of ESO are suggested for future analysis.

https://doi.org/10.5194/wes-2026-136
Preprint. Discussion started: 7 August 2026
© Author(s) 2026. CC BY 4.0 License.

6 Conclusion

The current study aims to quantify uncertainties related to assessment of EoI and ESO efficiency based on different types of meteorological observations. Five time series of joint precipitation and wind speed distributions at the Risø site in Denmark form base for the study.

The 10-minute temporal-resolution observations from the rain gauge and cup anemometer, spanning 19 years with ~5% missing data, are used to assess the uncertainty of shorter or longer time series for EoI. EoI results show high uncertainty for short time series, with differences of up to 170% between the minimum and maximum EoI values based on one year of data. Using a 10-year time series, the uncertainty in EoI is ~12% between the 25th and 75th percentiles. Median EoI is consistently shorter than the mean EoI due to a skewed distribution, with long EoI most pronounced in the short time series. Short EoI corresponds to much damage caused by heavy precipitation during high winds, while long EoI corresponds to little damage from limited precipitation in high winds. The Spearman coefficient for the joint wind speed and precipitation observations consistently takes positive values across all years and time series. Uncertainty in EoI due to the choice of droplet slowdown is ~24% when comparing an advanced model and the DNV RP.

IMERG satellite-based precipitation from 10 years combined with NEWA wind speeds, with 30-minute temporal resolution and ~0% missing data, provide EoI shorter than rain gauge, ~30% difference. IMERG and NEWA show higher Spearman coefficient than rain gauge and cup anemometer, which may explain the shorter EoI for IMERG.

High-frequency observations of precipitation from three disdrometers and wind speed from sonic anemometers at 1-minute temporal resolution, with ~25% missing data and short time series (1 to 3 years), are analyzed. Missing data and under catch of the disdrometer compared to the rain gauge and IMERG result in a positively biased EoI. EoI varies among the three disdrometers, ~20% difference.

Probabilistic variations in EoI are assessed across the five time-series by using Monte Carlo simulation calculating Pareto fronts. For normal operation, the turbines are not curtailed due to heavy precipitation. EoI varies for rain gauge from ~2 to ~7 years, for IMERG from ~2 to ~6 years, and for disdrometer from ~2 to ~8 years, based on three years of observations. Uncertainty due to material is larger than that due to weather, which may in part explain the good correspondence in EoI results across the different meteorological data types. The results support the field observation that damage levels may vary greatly between blades within a turbine and across a wind farm.

ESO efficiency is affected by the choice of droplet slowdown model, with the advanced model yielding flatter Pareto fronts. A flat Pareto front indicates high ESO efficiency, with only a small amount of AEP lost to ensure a long EoI extension. High-frequency data show flatter Pareto fronts than lower resolution data. Resampling disdrometer data from 1-minute to 30-minute intervals results in steeper Pareto fronts, as expected, similar to those of IMERG.

An unexpected finding is the flat Pareto front curve from the rain gauge, which crosses the disdrometer curve at 0.6% AEP loss. If taken at face value, it means very high ESO efficiency. However, a critical assessment of measurement qualities among

https://doi.org/10.5194/wes-2026-136
Preprint. Discussion started: 7 August 2026
© Author(s) 2026. CC BY 4.0 License.

rain gauge, disdrometer, and IMERG shows that the rain gauge, with a 1.2 mm h^{-1} measurement resolution, fails to capture precipitation details. Disdrometer and IMERG have a measurement resolution of 0.1 mm h^{-1}. The two disdrometers observing at the ground show similar steepness of Pareto fronts and variation. In contrast, the top-mounted disdrometer at 123 m shows a flatter curve and a larger spread, most likely due to under catch and/or a droplet-size distribution with smaller droplets than those observed at the ground.

Key take aways:

Long-term rain gauge and IMERG observations are suitable for assessing EoI, whereas disdrometer observations, which are prone to under catch, missing data, and short time series, are inadequate. Ten or more years are recommended for EoI assessment, and an advanced droplet slowdown model is recommended.

ESO efficiency is assessed in greater detail using disdrometer observations than with IMERG. Rain gauge observations are inadequate due to limited measurement resolution. Disdrometer observations show flatter Pareto fronts, indicating greater benefit from ESO, with lower AEP loss and a longer EoI extension than IMERG.

The synergy between long-term series and high-frequency observations is as follows: Long-term observations provide EoI and probabilistic variability, which jointly enable the ESO design criteria. Is ESO relevant at all? How many turbines need EoI extension, and for how long? High-frequency observations provide answers to ESO efficiency and operational conditions.

Appendix A

The uncertainty on EoI and ESO efficiency from wind speed extrapolation is tested based on cup anemometer wind speeds observed at 118 m and 125 m for 14 years (2012 to 2025) and extrapolated to 119 m combined with concurrent rain gauge data. Fig. A1 shows the yearly wind speeds and EoI for DTU 10 MW turbine. Fig. A2 shows Pareto fronts. In summary, EoI is 15.5 years using 118m wind speed data (assuming 118 m hub height), 14.4 years for 125m wind speed data (assuming 125 m hub height) and 14.7 years for extrapolated wind speeds from 125 m to 119 m (assuming 119 m hub height).

https://doi.org/10.5194/wes-2026-136
Preprint. Discussion started: 7 August 2026
© Author(s) 2026. CC BY 4.0 License.

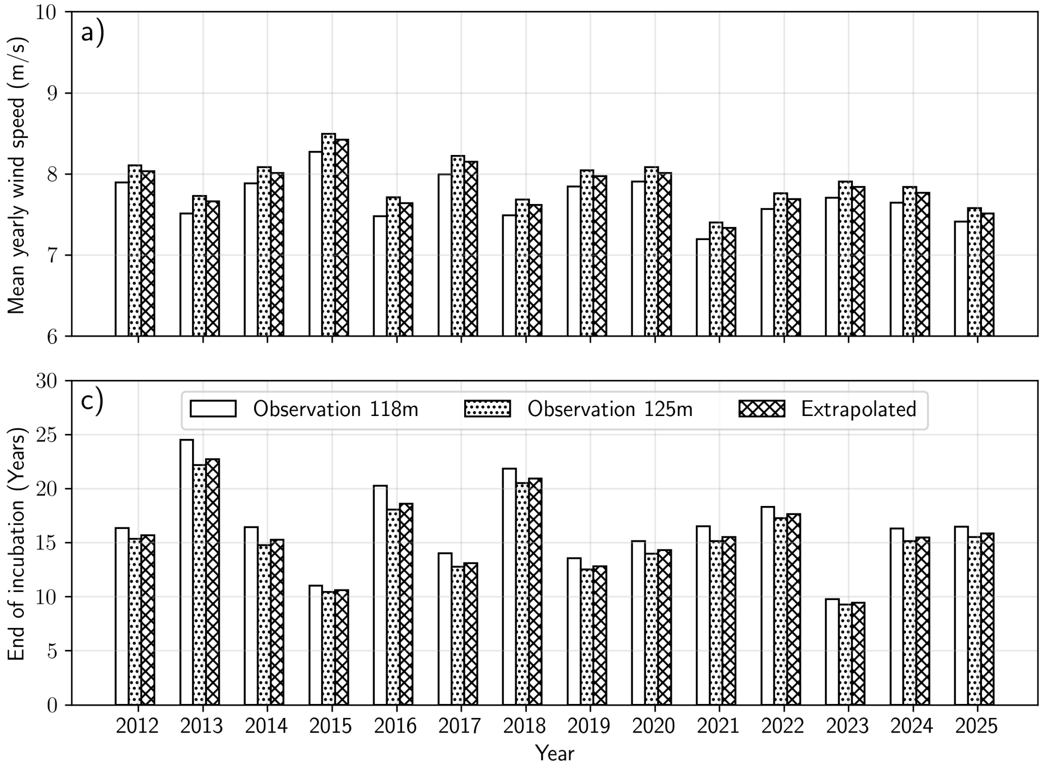

Fig. A1. a) Yearly average wind speed observed at 118 m and 125 m and extrapolated to 119 m. b) End of incubation per year for
695 DTU 10 MW turbine based on the wind speed input.

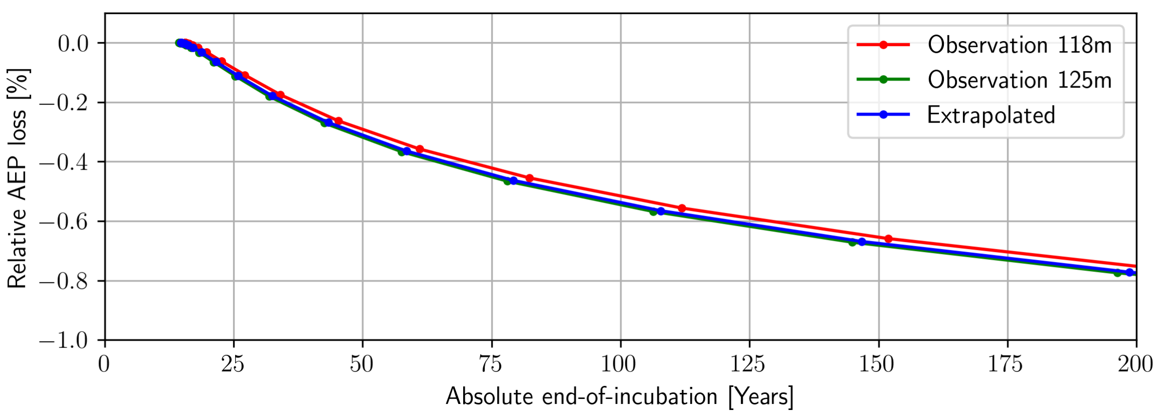

Fig. A2. ESO Pareto front for same weather data and turbine presented in Fig. A1.

© Author(s) 2026. CC BY 4.0 License.

Code and data availability

Code availability. The code is available at https://zenodo.org/records/17414783.
Data availability. The local observations at Risø campus are accessible from DTU Wind and Energy Systems. NEWA data are accessible from www.neweuropeanwindatlas.eu. IMERG data are accessible from https://gpm.nasa.gov/data/imerg.

Author contributions

Author contributions. CBH writing — original draft, Methodology, Funding acquisition, Conceptualization, Visualization, Fig. 2. AV writing—review and editing, Methodology, Data analysis, Visualization, Figs. 3-13 and A1 and A2. LDDST writing — review and editing, Visualization, Fig. 1. KD writing—review and editing. All authors have read and agreed to the published version of the manuscript.

Competing interests

The authors declare no conflict of interest.

Disclaimer

Copernicus Publications remains neutral with regard to jurisdictional claims made in the text, published maps, institutional affiliations, or any other geographical representation in this paper. While Copernicus Publications makes every effort to include appropriate place names, the final responsibility lies with the authors. Views expressed in the text are those of the authors and do not necessarily reflect the views of the publisher

Acknowledgements

We acknowledge the Goddard Earth Sciences Data and Information Services Center (GES DISC) for the GPM IMERG Final Precipitation product (Huffman et al., 2020). Wind speed data are obtained from the "New European Wind Atlas, a free, web-based application developed, owned, and operated by the NEWA. We thank the NEWA team for their support in extracting wind speed data. We gratefully acknowledge the computational and data resources provided on the Sophia HPC Cluster at the Technical University of Denmark, DOI: 10.57940/FAFC-6M81. We also thank Jens Visbech Madsen very warmly for his immense support and for developing the code.

© Author(s) 2026. CC BY 4.0 License.

Financial support

This work is supported by the AIRE project, which has received funding from the European Union under the grant agreement 101083716.

References

ASTM International: Standard test method for liquid impingement erosion using rotating apparatus. ASTM: Tech. Rep. ASTM G73-10, https://compass.astm.org/document/?contentCode=ASTM%7CG0073-10R21%7Cen-US, 2021.

Badger, M., Zuo, H., Hannesdóttir, Á., Owda, A., Hasager, C.: Lifetime prediction of turbine blades using global precipitation products from satellites, Wind Energ. Sci, 7, 2497–2512, https://doi.org/10.5194/wes-7-2497-2022, 2022.

Bak, C., Zahle, F., Bitsche, R., Kim, T., Yde, A., Henriksen, L. C., Andersen, P. B., Natarajan, A., Hansen, M. H.: Description of the DTU 10 MW Reference Wind Turbine. DTU Wind Energy Report-I-0092, Roskilde, Denmark, https://www.hawc2.dk/models/dtu-10-mw, 2013.

Barfknecht, N., von Terzi, D.: Aerodynamic interaction of rain and wind turbine blades: the significance of droplet slowdown and deformation for leading-edge erosion, Wind Energ. Sci., 9, 2333–2357, https://doi.org/10.5194/wes-9-2333-2024, 2024.

Barfknecht, N., Imhoff, R., Von Terzi, D.: Mitigating blade erosion damage through nowcast driven erosion safe mode control, Journal of Physics: Conference Series, 2767.3, 032001, https://iopscience.iop.org/article/10.1088/1742-6596/2767/3/032001, 2024.

Bartolomé, L., Teuwen, J.: Methodology for the energetic characterisation of rain erosion on wind turbine blades using meteorological data: A case study for The Netherlands, Wind Energy, 24, 686–698, https://doi.org/10.1002/we.2597, 2021.

Bech, J. I., Hasager, C. B., Bak, C.: Extending the life of wind turbine blade leading edges by reducing the tip speed during extreme precipitation events, Wind Energy Sci., 3(2), 729-748, https://doi.org/10.5194/wes-3-729-2018, 2018.

Bech, J. I., Johansen, N. F., Madsen, M. B., Hannesdóttir, Á., Hasager, C. B.: Experimental study on the effect of drop size in rain erosion test and on lifetime prediction of wind turbine blades, Renew. Energy, 197, 776–789, https://doi.org/10.1016/j.renene.2022.06.127, 2022.

Bechmann, A., Quick, J.: Market-Driven Wind Resource Assessment, Journal of Physics: Conference Series, 3025, 01200, https://iopscience.iop.org/article/10.1088/1742-6596/3025/1/012001/pdf, 2025.

Best, A.: The size distribution of raindrops, Q. J. R. Meteorol. Soc., 76, 16–36, https://doi.org/10.1002/qj.49707632704, 1950.

Caboni, M., van Dalum, G.: Developing an atlas of rain-induced leading edge erosion for wind turbine blades in the Dutch North Sea, Wind Energ. Sci., 10, 1887–1906, https://doi.org/10.5194/wes-10-1887-2025, 2025.

Caboni, M., Slot, H. M., Bergman, G., Wouters, D. A. J., Meijer, H. J. V. D. M.: Evaluation of wind turbine blades' rain-induced leading edge erosion using rainfall measurements at offshore, coastal and onshore locations in the Netherlands, Journal of Physics, 2767, https://doi.org/10.1088/1742-6596/2767/6/062003, 2024.

https://doi.org/10.5194/wes-2026-136
Preprint. Discussion started: 7 August 2026
© Author(s) 2026. CC BY 4.0 License.

Campobasso, M. S., Castorrini, A., Ortolani, A., Minisci, E.: Probabilistic analysis of wind turbine performance degradation due to blade erosion accounting for uncertainty of damage geometry, Renew. Sustain. Energy Rev., 178, 113254, https://doi.org/10.1016/j.rser.2023.113254, 2023.

Campobasso, M. S., Rose, M. S., Shende, S., Adirosi, E., Pace, G., Silvestri, L. D., Dimitriadou, K., Vinod, A., Hasager, C. B., Sánchez, F., Castorrini, A.: Development, performance and energy trade-off analyses of wind turbine precipitation-reactive control at offshore and onshore sites in Western Europe, Renew. Energy, 262, 25357, https://doi.org/10.1016/j.renene.2026.125357, 2026.

Castorrini, A., Barnabei, V. F., Domenech, L., Šakalyté, A., Sánchez, F., Campobasso, M. S.: Impact of meteorological data factors and material characterization method on the predictions of leading edge erosion of wind turbine blades, Renew. Energy, 227, https://doi.org/10.1016/j.renene.2024.120549, 2024.

Cornes, R. C., van den Schrier, G., van den Besselaar, E. J. M., Jones, P. D.: An ensemble version of the E-OBS temperature and precipitation data sets, J. Geophys. Res. Atmos.,123, 9391–9409, https://doi.org/10.1029/2017JD028200, 2018.

Dimitriadou, K., Hasager, C. B.: Comparison of GPM IMERG V07B versus IMERG V06B Precipitation in Northern Spain and their application for wind turbine blade lifetime estimation, Science of Remote Sensing, 4, 100458, https://doi.org/10.1016/j.srs.2026.100458, 2026.

Dimitriadou, K., Hasager, C. B., Nouqueret, E. C., Hannesdóttir, Á.: Quality assessment of the GPM IMERG product for lifetime prediction of turbine blades in complex terrain, J. Phys.: Conf. Ser., 2767, 042010, https://doi.org/10.1088/1742-6596/2767/4/042010, 2024.

DMI: Klimastatus 2025, DMI Report 25-15, https://www.dmi.dk/fileadmin/NCKF/Rapporter/NCKF_-_Klimastatus_2025.pdf, (in Danish) 2025.

DNV: DNV-RP-0573 Evaluation of Erosion and Delamination for Leading Edge Protection Systems of Rotor Blades, Det Norske Veritas: Høvik, Norway, 2021.

Dörenkämper, M., Olsen, B. T., Witha, B., Hahmann, A. N., Davis, N. N., Barcons, J., Ezber, Y., García-Bustamante, E., González-Rouco, J. F., Navarro, J., Sastre-Marugán, M., Sīle, T., Trei, W., Žagar, M., Badger, J., Gottschall, J., Sanz Rodrigo, J., and Mann, J.: The Making of the New European Wind Atlas – Part 2: Production and evaluation, Geosci. Model Dev., 13, 5079–5102, https://doi.org/10.5194/gmd-13-5079-2020, 2020.

EMBER: Wind and solar generated more power than fossil fuels in the EU for the first time in 2025, https://ember-energy.org/latest-updates/wind-and-solar-generated-more-power-than-fossil-fuels-in-the-eu-for-the-first-time-in-2025/, 2026.

Forsting, A. M., Dicholkar, A., Sørensen, N. N., Olsen, A. S., Bak, C., Theron, J. N., Aihara, A., Caboni, M., Ravishankara, A. K., Vimalakanthan, K., Bretos, D., Mendez, B., Campaña-Alonso, G., Jimenez, O. P., Grasso, F., Campobasso, M. S., Maniaci, D.: Benchmarking aerodynamic codes for 2D aerofoils with leading edge erosion, IOP Publishing, 042037, https://doi.org/10.1088/1742-6596/3224/4/042037, 2026.

© Author(s) 2026. CC BY 4.0 License.

Gaertner, E., Rinker, J., Sethuraman, L., Zahle, F., Anderson, B., Barter, G., Abbas, N., Meng, F., Bortolotti, P., Skrzypinski, W., et al.: Definition of the IEA Wind 15-Megawatt Offshore Reference Wind Turbine, IEA Wind TCP Task 37 Technical Report, National Renewable Energy Laboratory (NREL): Golden, CO, USA, http://dx.doi.org/10.2172/1603478, 2020.

Gao, L., Chen, J., Zhang, Y., Zhang, L., Mao, X.: Evaluation of TPMFD and CRA/Land Precipitation Data Performance Compared to IMERG V07 on the Tibetan Plateau Using Non-CMA Stations, Atmos. Res., 322, 108123, https://doi.org/10.1016/j.atmosres.2025.108123, 2025.

Ghiggi, G., Candolfi, K., Billaux-Roux, A.-C., Longchamps, R., Pham-Ba, S., Weil, C., Berne, A.: Disdrodb: an open-source Python package for standardized processing, sharing, and analysis of disdrometer data, EGUsphere [preprint], https://doi.org/10.5194/egusphere-2026-1886, 2026.

GPCC: Global Precipitation Climatology Centre, https://climatedataguide.ucar.edu/climate-data/gpcc-global-precipitation-climatology-centre, 2026.

GWEC: Global Wind Report 2025, Global Wind Energy Council: Brussels, Belgium, https://gwec.net/reports/, 2025.

Haakenstad, H., Breivik, Ø., Furevik, B. R., Reistad, M., Bohlinger, P., Aarnes, P. O. J.: NORA3: A Nonhydrostatic High-Resolution Hindcast of the North Sea, the Norwegian Sea, and the Barents Sea, J. Appl. Meteorol. Climatol., 60, 1443–1464, https://doi.org/10.1175/JAMC-D-21-0029.1, 2021.

Hannesdóttir, Á., Dellwik, E., Hasager, C. B.: Prediction of rain erosion damage progression using disdrometer rain data: The importance of liquid water content, J. Phys.: Conf. Ser., 2767 04202, https://doi.org/10.1088/1742-6596/2767/4/042024, 2024b.

Hannesdóttir, Á., Kral, S.T., Reuder, J., Hasager, C. B.: Rain erosion atlas for wind turbine blades based on ERA5 and NORA3 for Scandinavia, Results Eng., 22, 102010, https://doi.org/10.1016/j.rineng.2024.102010, 2024a.

Hasager, C., Vejen, F., Bech, J., Skrzypiński, W., Tilg, A.-M., Nielsen, M.: Assessment of the rain and wind climate with focus on wind turbine blade leading edge erosion rate and expected lifetime in Danish Seas, Renew. Energy, 149, 91–102, https://doi.org/10.1016/j.renene.2019.12.043, 2020.

Hasager, C. B., Vejen, F., Skrzypiński, W. R., Tilg, A.-M.: Rain Erosion Load and Its Effect on Leading-Edge Lifetime and Potential of Erosion-Safe Mode at Wind Turbines in the North Sea and Baltic Sea, Energies, 14(7), 1959, https://doi.org/10.3390/en14071959, 2021.

Hersbach, H., Bell, B., Berrisford, P., Hirahara, S., Horányi, A., Muñoz-Sabater, J., Nicolas, J., Peubey, C., Radu, R., Schepers, D., et al.: The ERA5 global reanalysis, Q. J. R. Meteorol. Soc., 146, 1999–2049, https://doi.org/10.1002/qj.3803, 2020.

Huffman, G.J., Bolvin, D. T., Nelkin, E. J., Wolff, D. B., Adler, R. F., Gu, G., Hong, Y., Bowman, K. P., Stocker, E. F.: Integrated Multi-satellite Retrievals for the Global Precipitation Measurement (GPM) Mission (IMERG), In Satellite Precipitation Measurement; Levizzani, V., Kidd, C., Kirschbaum, D. B., Kummerow, C. D., Nakamura, K., Turk, F. J., Eds., Springer: Cham, 67, pp. 343–353. https://doi.org/10.1007/978-3-030-24568-9_19, 2020.

https://doi.org/10.5194/wes-2026-136
Preprint. Discussion started: 7 August 2026
© Author(s) 2026. CC BY 4.0 License.

Huffman, G. J., Bolvin, D. T., Joyce, R., Kelley, O. A., Nelkin, E. J., Tan, J., Watters, D. C., West, B. J.: Integrated Multi-satellitE Retrievals for GPM (IMERG) Technical Documentation, Technical Report, NASA Goddard Space Flight Center, https://gpm.nasa.gov/sites/default/files/2023-07/IMERG_TechnicalDocumentation_final_230713.pdf, 2023.

Jonkman, J., Butterfield, S., Musial, W., Scott, G.: Definition of A 5-MW Reference Wind Turbine for Offshore System Development, Technical Report NREL/TP-500-38060, National Renewable Energy Laboratory (NREL): Golden, CO, USA, http://dx.doi.org/10.2172/947422, 2009.

Letson, F., Pryor, S. C.: From Hydrometeor Size Distribution Measurements to Projections of Wind Turbine Blade Leading-Edge Erosion, Energies, 16(9), 3906, https://doi.org/10.3390/en16093906, 2023.

Madsen, J. V., Hannesdóttir, Á., Vinod, A., Hasager, C. B.: D4.5- Erosion-safe operation design tool: Dedicated Toolbox Design, AIRE, https://backend.orbit.dtu.dk/ws/portalfiles/portal/439284563/AIRE_D4_5CurtailmentStrategyTool_1_.pdf, 2026.

Malik, T. H., Bak, C.: Challenges in detecting wind turbine power loss: the effects of blade erosion, turbulence, and time averaging, Wind Energ. Sci., 10, 227–243, https://doi.org/10.5194/wes-10-227-2025, 2025.

Maniaci, D. C., MacDonald, H., Paquette, J., Clarke, R.: Leading Edge Erosion Classification System, Technical Report from IEA Wind Task 46 Erosion of Wind Turbine Blades, Sandia National Lab: Albuquerque, NM, USA, https://iea-wind.org/wp-content/uploads/2023/02/IEA-Wind-Task-46-Erosion-Classification-System-report.pdf, 2022.

Maniaci, D., Forsting, A. M., Barlas, A., Bak, C., Olsen, A. S.: Model to predict annual energy production loss based on blade erosion class, Technical report, IEA Task 46, https://backend.orbit.dtu.dk/ws/portalfiles/portal/413479447/IEA_Wind_Task_46_WP3.1_AEP_Loss-1.pdf, 2025.

Marshall, J.S., Palmer, W. M. K.: The Distribution of Raindrops with Size, Journal of Meteorology, 5, 165-166, http://dx.doi.org/10.1175/1520-0469(1948)005<0165:TDORWS>2.0.CO;2, 1948.

Mishnaevsky Jr., L.: Repair of wind turbine blades: Review of methods and related computational mechanics problems, Renewable Energy,140, 828-839, https://doi.org/10.1016/j.renene.2019.03.113, 2019.

Mishnaevsky Jr., L., Hasager, C. B., Bak, C., Tilg, A.-M., Bech, J. I., Doagou Rad, S., Fæster, S.: Leading edge erosion of wind turbine blades: Understanding, prevention and protection, Renewable Energy, 169, 953-969, https://doi.org/10.1016/j.renene.2021.01.044, 2021.

Mishnaevsky, L., Jr., Tempelis, A., Belahurau, Y., Johansen, N. F.-J.: Microplastics Emission from Eroding Wind Turbine Blades: Preliminary Estimations of Volume, Energies, 17, 6260, https://doi.org/10.3390/en17246260, 2024.

Mishnaevsky Jr, L., Thomsen, K.: Costs of repair of wind turbine blades: Influence of technology aspects, Wind Energy, 23, 2247–2255, https://doi.org/10.1002/we.2552, 2020.

NCAR Staff: National Center for Atmospheric Research Staff (Eds). Last modified 2025-12-11 "The Climate Data Guide: GPCC: Global Precipitation Climatology Centre, https://climatedataguide.ucar.edu/climate-data/gpcc-global-precipitation-climatology-centre, 2026.

NEWA: New European Wind Atlas, DTU, Roskilde, Denmark, https://www.neweuropeanwindatlas.eu/, 2026.

https://doi.org/10.5194/wes-2026-136
Preprint. Discussion started: 7 August 2026
© Author(s) 2026. CC BY 4.0 License.

Papadakis, M., Wong, S.-C., Rachman, A., Hung, K. E., Vu, G. T., Bidwell, C. S.: Large and Small Droplet Impingement Data on Airfoils and Two Simulated Ice Shapes, NASA, Report #E-15275, Glenn Research Center: Cleveland, OH, USA, https://ntrs.nasa.gov/citations/20070034950, 2007.

Punge, H. J., Kunz, M.: Hail observations and hailstorm characteristics in Europe: A review, Atmospheric Research, 176–177,159-184. https://doi.org/10.1016/j.atmosres.2016.02.012, 2016.

Pradhan, R. K., Markonis, Y., Vargas Godoy, M. R., Villalba-Pradas, A., Andreadis, K.M., Nikolopoulos, E.I., Papalexiou, S. M., Rahim, A., Tapiador, F. J., Hanel, M.: Review of GPM IMERG Performance: A Global Perspective, Remote Sens. Environ., 268, 112754, https://doi.org/10.1016/j.rse.2021.112754, 2022.

Prieto, R., Karlsson T.: A model to estimate the effect of variables causing erosion in wind turbine blades, Wind Energy, 24,1031–1044, https://doi.org/10.1002/we.2615, 2021.

Pryor, S. C., Barthelmie, R. J.: Hail as a damage vector for renewable energy, IScience, 29, https://doi.org/10.1016/j.isci.2025.114439, 2026.

Pryor, S. C., Coburn, J. J., Barthelmie, R. J.: Spatiotemporal Variability in Wind Turbine Blade Leading Edge Erosion, Energies, 18(2), 425, https://doi.org/10.3390/en18020425, 2025.

Sakai, E., Hashimoto, A., Nanko, K., Takahashi, T., Nishida, H., Tamura, H., Hattori, Y., Kitano, Y.: Rain Erosion Atlas of Wind Turbine Blades for Japan Based on Long-Term Meteorological and Climate Dataset CRIEPI-RCM-Era2, Wind,, 6, 7, https://doi.org/10.3390/wind6010007, 2026.

Sánchez, F., Hao, H., Domenech, L., Hardalupas, Y., Dyer, K., García-Peñas, V., Charalambides, M., Ibáñez-Arnal, M., Sergis, A., Taylor, A. M. K. P.: Rain erosion damage initiation assessment of wind turbine blades leading edge protection systems based on laboratory testing data: a review and case study, Results in Engineering, 30, 110327, https://doi.org/10.1016/j.rineng.2026.110327, 2026.

Simon, J. E., Bajpai, A., Johansen, N. F.-J., Hannesdóttir, Á., Hasager, C.: Lifetime estimation of blade erosion using rain erosion test data with different analysis methods, Wind Energy (accepted), 2026.

Skrzypiński, W. R., Bech, J. I., Hasager, C. B., Tilg, A.-M., Vejen, F., Bak, C.: Optimization of the erosion-safe operation of the IEA Wind 15 MW Reference Wind Turbine, J. Phys.: Conf. Ser, 1618, 052034. https://iopscience.iop.org/article/10.1088/1742-6596/1618/5/052034, 2020.

Springer, G.S.: Erosion by Liquid Impact, John Wiley and Sons: New York, NY, USA, p. 278, 1976.

Solbrekke, I.M., Sorteberg, A., Haakenstad, H.: The 3 km Norwegian reanalysis (NORA3) – a validation of offshore wind resources in the North Sea and the Norwegian Sea, Wind Energy Sci., 6, 1501–1519, https://doi.org/10.5194/wes-6-1501-2021, 2021.

Tilg, A.-M., Hasager, C. B., Kirtzel, H.-J., Hummelshøj, P.: Brief communication: Nowcasting of precipitation for leading-edge-erosion-safe mode, Wind Energ. Sci. 5, 977–981, https://doi.org/10.5194/wes-5-977-2020, 2020.

https://doi.org/10.5194/wes-2026-136
Preprint. Discussion started: 7 August 2026
© Author(s) 2026. CC BY 4.0 License.

Verma, A. S., Jiang, Z., Ren, Z., Caboni, M., Verhoef, H., Mijle Meijer, H. v. d., Castro, S. G. P., Teuwen, J. J. E.: A probabilistic long-term framework for site-specific erosion analysis of wind turbine blades: A case study of 31 Dutch sites, Wind Energy, 24,1314–1336, https://doi.org/10.1002/we.2634, 2021a.

Verma, A. S., Jiang, Z., Caboni, M., Verhoef, H., Milje Meijer, H. v. d., Castro, S. G. P., Teuwen, J. J. E.: A probabilistic rainfall model to estimate the leading-edge lifetime of wind turbine blade coating system, Renew. Energy, 178, 435-1455, https://doi.org/10.1016/j.renene.2021.06.125, 2021b.

Visbech, J., Göçmen, T., Hasager, C. B., Shkalov, H., Handberg, M., Nielsen, K. P.: Introducing a data-driven approach to predict site-specific leading-edge erosion from mesoscale weather simulations, Wind. Energy Sci., 8,173–191, http://dx.doi.org/10.5194/wes-8-173-2023, 2023.

Visbech, J., Göçmen, T., Özçakmak, Ö. S., Forsting, A. M., Hannesdóttir, Á., Réthoré, P. -E.: Aerodynamic effects of leading-edge erosion in wind farm flow modeling, Wind Energy Sci., 9, 1811-1826, https://doi.org/10.5194/wes-9-1811-2024, 2024b.

Visbech, J., Göçmen, T., Réthoré, P. - E., Hasager, C. B.: Erosion-safe operation using double deep Q-learning, J. Phys.: Conf. Ser., 2767, 032047, https://iopscience.iop.org/article/10.1088/1742-6596/2767/3/032047, 2024a.

Visbech, J., Hasager, C. B., Göçmen, T., Réthoré, P. - E.: Copula-based joint distributions of rain and wind for leading edge erosion risk atlas, Renew. Energy, 253,123358, https://doi.org/10.1016/j.renene.2025.123358, 2025.

Wang, J., Wolff, D. B., Tan, J., Marks, D. A., Pippitt, J. L., Huffman, G. J.: Validation of IMERG Oceanic Precipitation over Kwajalein, Remote Sens., 14, 3753, https://doi.org/10.3390/rs14153753, 2022.

Yu, L., Leng, G., Python, A.: A Comprehensive Validation for GPM IMERG Precipitation Products to Detect Extremes and Drought over Mainland China, Weather Clim. Extrem., 36, 100458, https://doi.org/10.1016/j.wace.2022.100458, 2022.

Xiong, W., Tang, G., Wang, T., Ma, Z., Wan, W.: Evaluation of IMERG and ERA5 Precipitation-Phase Partitioning on the Global Scale, Water, 14, 1122, https://doi.org/10.3390/w14071122, 2022.